The allometry of oxygen supply and demand in the California Horn Shark, *Heterodontus francisci*

by

Tanya Sarah Prinzing

B.Sc. Biology Simon Fraser University, 2017

Thesis Submitted in Partial Fulfillment of the
Requirements for the Degree of
Master of Science

in the
Department of Biological Sciences
Faculty of Science

SIMON FRASER UNIVERSITY
Spring 2021

Declaration of Committee

Name:	**Tanya S. Prinzing**
Degree:	**Master of Science (Biological Sciences)**
Thesis title:	**The allometry of oxygen supply and demand in the California Horn Shark, *Heterodontus francisci***
Committee:	**Chair:** Jim Mattsson Associate Professor, Biological Sciences
	Nicholas Dulvy Supervisor Professor, Biological Sciences
	Tony Williams Committee Member Professor, Biological Sciences
	Shaun Killen Examiner Professor, Biodiversity, Animal Health & Comparative Medicine University of Glasgow

Ethics Statement

The author, whose name appears on the title page of this work, has obtained, for the research described in this work, either:

a. human research ethics approval from the Simon Fraser University Office of Research Ethics

or

b. advance approval of the animal care protocol from the University Animal Care Committee of Simon Fraser University

or has conducted the research

c. as a co-investigator, collaborator, or research assistant in a research project approved in advance.

A copy of the approval letter has been filed with the Theses Office of the University Library at the time of submission of this thesis or project.

The original application for approval and letter of approval are filed with the relevant offices. Inquiries may be directed to those authorities.

Simon Fraser University Library
Burnaby, British Columbia, Canada

Update Spring 2016

Abstract

The scaling relationship between metabolic rate and body mass is one of the most notable functional relationships in comparative physiology and macroecology. In aquatic ectotherms, the surface area of the gills is thought to be a major contributor to the allometric scaling patterns we see for metabolic rate, both within and across species. Here, I first examined the allometric relationship between oxygen supply (gill area) and consumption (metabolic rate) and found that the allometry of gill area was isometric and very similar to that of metabolic rate. Second, I tested the effects of three statistical analysis techniques for estimating maximum metabolic rate and found that a rolling regression model was the best candidate model across four fish species. Together, these results support the hypothesis that oxygen supply and demand are closely matched and suggest that a two-dimensional gill can overcome geometric constraints to increase at the same rate as the three-dimensional mass of an inactive organism. Additionally, they highlight the importance of statistical choices in producing comparable and reproducible estimates of metabolic rate across species.

Keywords: allometry; California Horn Shark; gill surface area; maximum metabolic rate; statistical analysis; surface area-to-volume constraints

Acknowledgements

This research would not have been possible without the help and support of many clever, motivational, kind and generous individuals.

First, I want to thank Nick Dulvy for taking me on as a student, staring me on this journey and allowing me to take on a project that has been as fulfilling as this one. I appreciate the time you've taken to critique my work and provide helpful feedback. A big thank you to Tony Williams for being a great committee member. Your calm demeanor, patience, support and perspective have been invaluable, and this research is far better because you were a part of it. Thank you for looking past our fishy ways to provide such helpful feedback.

I am forever indebted to the amazing crew at Southwest Fisheries Science Center in La Jolla, California, where the majority of the data collection for this research took place. Nick Wegner, Kathy Swiney, Garrett Seibert, Steph Nemeth, Joshua Lonthair, and of course Zach Skelton, thank you for making this work possible by generously giving your time, expertise, and sanity to help me wrangle all those sharks. I feel lucky to have gained such amazing colleagues and friends. Zach, thank you for taking me under your wing to teach me how to get all the bubbles out and endlessly accommodate my somewhat ridiculous late-night shark hunting requests. Nick, thank you for taking a chance on hosting a fish-secret stealing Canadian spy and making this research possible. Your patience as I made mistakes helped me believe I would indeed figure it out and everything would work out great. I am immensely grateful for the time you've taken to critique my arguments, talk through ideas, and just have fun. I am a much better writer and scientist for it. Also, to Chiara Fresia, thank you for working so hard to make our stay so memorable and being one of the best people I know. I will always remember what vegan gluten-free gnocchi taste like thanks to your kind and loving nature.

It has been a privilege to complete this journey alongside the wonderful scientists of SFU Biology, E2O, and the Dulvy lab. Your feedback and support in developing presentations, statistical analyses, and writing has been invaluable, and as a bonus, you all happen to be a hilarious and wonderful group of people always ready for a

decompressing hang out or craft night. A special thank you to Gill Gang members Jenny Bigman and Serena Wong for helping me find my footing and develop my project all while keeping things in perspective. I learned so much from you and am so grateful I was able to share this experience with you. Also, thank you to Yangfan Zhang for taking the time to talk through ideas until we figured everything out, it was a pleasure getting to work with you and I learned so much from you.

The last thank you goes to my family and friends. Marcus, thank you for believing in me when I didn't, telling me there was a light on the other side, and encouraging me to push just a little harder. Your love and support have helped me learn to be proud of what I have achieved even if it's not perfect. To my parents, thank you for supporting me, listening to my ramblings as I struggled to make sense of my work, and instilling in me an innate need to seek out challenges and never be satisfied, just the qualities I needed to succeed at this degree. To my father, you have made me into the independent, overly critical, and endlessly curious person I am today, and I am forever grateful for it.

Table of Contents

List of Tables

List of Figures

List of Acronyms

RMR	Resting metabolic rate
MMR	Maximum metabolic rate
SD	Standard Deviation
CI	95% Confidence Interval

Chapter 1.

Introduction

Energy is universal to all ecosystems on earth. All organisms must uptake and allocate energy to the processes of growth, survival, and reproduction by way of their metabolic rate. Thus, metabolic rate may offer a quantifiable way to connect processes occurring across species and ecosystems, which is a key goal of the field of ecology as a whole (Brown et al. 2004; Burger et al., 2019). By understanding how energy is used and transferred across species, we may be able to get a picture of those species' contribution to their ecosystem to inform conservation initiatives and make predictions of the impacts of climate change (Schramski et al., 2015). However, just as how we see high levels of complexity within and across ecosystems, metabolism has proven difficult to generalize. The rate of oxygen consumption (M_{O_2}) is used as a proxy for metabolic rate following a power law relationship, $M_{O_2} = aM^b$, where a is the species-specific coefficient, M is body mass, and b is the scaling exponent or slope of the relationship on a log-log scale. It is widely accepted that the amount of energy used by an organism varies with body mass, temperature, and other ecological factors across species (Burton et al., 2011; Clarke and Johnston, 1999; Glazier, 2005). Whether variation in b is statistical noise or is related to ecological traits is hotly debated and the mechanisms underlying this variation are still not well understood (Killen et al., 2010). However, variation in b has been linked to activity level, metabolic level, and lifestyle, such that values of b are greater during periods of strenuous activity as well as in species which place relatively little demand on their surface areas (Glazier, 2005; Killen et al., 2010).

There is growing interest in uncovering the broad-scale morphological and physiological factors that may help shape the relationship between metabolic rate and body mass, such as respiratory surface area (Gillooly et al., 2016; Killen et al., 2016; Pauly, 2010). In aquatic ectotherms such as fish, the surface area of the gills acts as the exchange surface for gasses, metabolites, and waste products between the animal and its surrounding environment. Thus, gill area is closely tied to metabolic rate, and may be a key component of a holistic understanding of its variation across species (De Jager and Dekkers, 1975; Hughes, 1972). Compared to metabolic rate, gill area is relatively

easy to measure and there are few restrictions on how large of an animal can be analyzed (Wegner, 2011; 2010). If the relationship between metabolic rate and gill area can be quantified, estimating gill area may be a more accessible method of inferring broad-scale patterns of metabolic rate and life histories across species. Though gill area is plastic and can be augmented in response to environmental stimuli, such as oxygen availability, it is relatively stable compared to metabolic rate, which is constantly changing with activity level (Chapman et al., 2000; Phuong et al., 2017). Importantly, if the allometric scaling of metabolic rate varies with activity level and lifestyle, gill area may act as a relatively stable indicator of the metabolic requirements of a species. For example, the high oxygen demands of active species such as a salmonids may result in gill surface area that more closely matches maximum metabolic rate, while the relatively low demands of a carp's lifestyle may lead to gill area closer to resting metabolic rate (Glazier, 2005; Hughes, 1984; Luo et al., 2020).

While using across-species, or inter-specific, analysis to examine the link between metabolic rate and gill area is extremely valuable (Gillooly et al., 2016; Killen et al., 2016), the resolution of within species, or intra-specific, analyses is required to help reveal the drivers of this relationship (e.g. Killen et al. 2010). Taking this a step further and estimating both metabolic rate and gill area in the same individual animals greatly reduces the confounding factor of individual variation and allows us to directly test how each trait is related to the other. Yet, there are extremely few studies which test the relationship between gill are and metabolic rate using a within-species approach, and none which test against metabolic rate at metabolic levels other than resting.

Quality analyses depend on quality data. Attention is increasingly being paid to the necessity of reproducible metabolic rate estimates if we are to make broad, across-species comparisons (Clark et al., 2013; Killen et al., 2017). However, while experimental methods have been undergoing a welcome refinement, the statistical analysis of maximum metabolic rate has received relatively little notice (Clark et al., 2013; Roche et al., 2013; Rummer et al., 2016). Estimates of maximum metabolic rate are required to characterize a species' aerobic scope, or capacity for energy expenditure above rest (Clark et al., 2013). There are two issues hindering the standardization of maximum metabolic rate analysis, namely few instructional resources and poor methods reporting in the literature. This leaves both novice and experienced researchers to rely on lab tradition or word of mouth when designing experimental analyses.

In Chapter 2, my first data chapter, I test the relationship between gill area and both resting and maximum metabolic rates using a near-complete body size range of an inactive coastal shark, the California Horn Shark (*Heterodontus francisci*). I asked (1) does the allometric scaling of metabolic rate vary with activity level, here between resting and maximum metabolic rate, and (2) is the slope of gill area nearer to that of resting or maximum metabolic rates, or neither? I found that the slope of maximum metabolic rate was hyperallometric (>1) and significantly steeper than the slope of resting metabolic rate, which was isometric (~1). Surprisingly, I found that a broken regression model was a better representation of the allometric slope of gill area and that the slope may shift at the transition from juvenile to adolescent developmental stages. When analyzed this way, the slope of gill area across adolescents and adults was isometric but not significantly different from the slopes of either maximum or resting metabolic rates. This steep scaling pattern suggests that gill area is not limited by surface area-to-volume constraints and can meet the metabolic needs of the animal; California Horn Shark are slow swimmers and spend a considerable amount of time at rest, likely leading to gills that reflect this lifestyle. However, we cannot exclude the possibility that metabolic rate is limited by the gill area available for gas exchange, where metabolic rate would be higher if the gills were larger.

In my second data chapter (Chapter 3), I expanded my experimental analysis to test which of the available statistical analysis methods produced the most precise and repeatable estimates of maximum metabolic rate across two shark and two salmonid species. I found that a rolling regression model with a short, 1- to 2-minute regression window was the best candidate model, as it was simple to use across the tested data types and required the least amount of subjectivity. These results can be used to help standardize the estimation of maximum metabolic rate and improve comparability across species.

I conclude my thesis with an overview of my key findings and a discussion of their implications for the analysis of metabolic rate across species. Overall, my thesis has been an exploration of some of the methods and assumptions that underly how we think about metabolic ecology, and this work contributes to the framework under which we can apply this theory in the future.

1.1. References

Brown, J. H., Gillooly, J. F., Allen, A. P., Savage, V. M. and West, G. B. (2004). Toward a metabolic theory of ecology. *Ecology* 85, 1771–1789.

Burger, J. R., Hou, C. and Brown, J. H. (2019). Toward a metabolic theory of life history. *Proc. Natl. Acad. Sci.* 116, 26653–26661.

Burton, T., Killen, S. S., Armstrong, J. D. and Metcalfe, N. B. (2011). What causes intraspecific variation in resting metabolic rate and what are its ecological consequences? *Proc. R. Soc. B Biol. Sci.* 278, 3465–3473.

Chapman, L. G., Galis, F. and Shinn, J. (2000). Phenotypic plasticity and the possible role of genetic assimilation: Hypoxia-induced trade-offs in the morphological traits of an African cichlid. *Ecol. Lett.* 3, 387–393.

Clark, T. D., Sandblom, E. and Jutfelt, F. (2013). Aerobic scope measurements of fishes in an era of climate change: respirometry, relevance and recommendations. *J. Exp. Biol.* 216, 2771–2782.

Clarke, A. and Johnston, N. M. (1999). Scaling of metabolic rate with body mass and temperature in teleost fish. *J. Anim. Ecol.* 68, 893–905.

De Jager, S. and Dekkers, W. (1975). Relations between gill structure and activity in fish. *Netherlands J. Zool.* 25, 276–308.

Gillooly, J. F., Gomez, J. P., Mavrodiev, E. V., Rong, Y. and McLamore, E. S. (2016). Body mass scaling of passive oxygen diffusion in endotherms and ectotherms. *Proc. Natl. Acad. Sci.* 113, 5340–5345.

Glazier, D. S. (2005). Beyond the “3/4-power law”: Variation in the intra- and interspecific scaling of metabolic rate in animals. *Biol. Rev. Camb. Philos. Soc.* 80, 611–662.

Hughes, G. M. (1972). Morphometrics of Fish Gills. In *Respiration Physiology*, pp. 1–25.

Hughes, G. M. (1984). Scaling of respiratory areas in relation to oxygen consumption of vertebrates. *Experientia* 40, 519–524.

Killen, S. S., Atkinson, D. and Glazier, D. S. (2010). The intraspecific scaling of metabolic rate with body mass in fishes depends on lifestyle and temperature. *Ecol. Lett.* 13, 184–193.

Killen, S. S., Glazier, D. S., Rezende, E. L., Clark, T. D., Atkinson, D., Willener, A. S. T. and Halsey, L. G. (2016). Ecological Influences and Morphological Correlates of Resting and Maximal Metabolic Rates across Teleost Fish Species. *Am. Nat.* 187, 592–606.

Killen, S. S., Norin, T. and Halsey, L. G. (2017). Do method and species lifestyle affect measures of maximum metabolic rate in fishes? *J. Fish Biol.* 90, 1037–1046.

Luo, Y., Li, Q., Zhu, X., Zhou, J., Shen, C., Xia, D., Djiba, P. K., Xie, H., Lv, X., Jia, J., et al. (2020). Ventilation frequency reveals the roles of exchange surface areas in metabolic scaling. *Physiol. Biochem. Zool.* 93, 13–22.

Pauly, D. (2010). Gasping fish and panting squids: Oxygen, temperature and the growth of water-breathing animals. *Excell. Ecol.* 22, 1–247.

Phuong, L. M., Huong, D. T. T., Nyengaard, J. R. and Bayley, M. (2017). Gill remodelling and growth rate of striped catfish Pangasianodon hypophthalmus under impacts of hypoxia and temperature. *Comp. Biochem. Physiol. -Part A Mol. Integr. Physiol.* 203, 288–296.

Roche, D. G., Binning, S. A., Bosiger, Y., Johansen, J. L. and Rummer, J. L. (2013). Finding the best estimates of metabolic rates in a coral reef fish. *J. Exp. Biol.* 216, 2103–2110.

Rummer, J. L., Binning, S. A., Roche, D. G. and Johansen, J. L. (2016). Methods matter: Considering locomotory mode and respirometry technique when estimating metabolic rates of fishes. *Conserv. Physiol.* 4, 1–13.

Savage, V. M., Gillooly, J. F., Woodruff, W. H., West, G. B., Allen, A. P., Enquist, B. J. and Brown, J. H. (2004). The predominance of quarter-power scaling in biology. *Funct. Ecol.* 18, 257–282.

Schramski, J. R., Dell, A. I., Grady, J. M., Sibly, R. M. and Brown, J. H. (2015). Metabolic theory predicts whole-ecosystem properties. *Proc. Natl. Acad. Sci. U. S. A.* 112, 2617–2622.

Wegner, N. C. (2011). *Gill Respiratory Morphometrics*. Elsevier Inc.

Wegner, N. C., Sepulveda, C. A., Bull, K. B. and Graham, J. B. (2010). Gill morphometrics in relation to gas transfer and ram ventilation in high-energy demand teleosts: Scombrids and billfishes. *J. Morphol.* 271, 36–49.

White, C. R., Phillips, N. F. and Seymour, R. S. (2006). The scaling and temperature dependence of vertebrate metabolism. *Biol. Lett.* 2, 125–127.

Chapter 2.

The allomeric scaling of oxygen supply and demand in California Horn Shark, *Heterodontus francisci*[1]

2.1. Abstract

In aquatic ectotherms, the surface area of the gills is hypothesized to be a major contributor to the metabolic scaling patterns observed across species, yet there are surprisingly few within-species ontogenetic tests of this hypothesis. Here, we examined the relationship between oxygen demand and supply by making paired estimates of maximum and resting metabolic rates as well as gill surface area across the full body size range of a small, relatively inactive coastal shark. We found that the allometric slope of maximum metabolic rate was hyper-allometric (1.079 ± 0.044 95% CI) and considerably steeper than the slope of resting metabolic rate (0.971 ± 0.064). Further, we found that a broken stick regression analysis better described the gill area data and revealed that the allometric scaling of gill area may shift during early adolescence to become isometric in adulthood (1.014 ± 0.151). Together, these results suggest that, in a relatively inactive species, metabolic rate may not be limited by the potential surface area-to-volume ratio constraints of gill area and can thus scale isometrically or above with body mass. However, this analysis cannot refute that a limitation may exist in, for example, a relatively active species. Future work should examine whether we find a pattern of relatively shallow allometric slopes in highly active fish species to help elucidate whether a constraint may indeed exist under the condition of very high oxygen demand.

[1] A version of this chapter is in preparation for journal submission with co-authors Jennifer S. Bigman, Zachary R. Skelton, Nicholas K. Dulvy, and Nicholas C. Wegner

2.2. Introduction

The change in or scaling of an organism's metabolic rate with body mass and the physiological underpinnings of this relationship are of great interest to physiologists and ecologists alike (Brown et al., 2004; Gillooly et al., 2016; Hughes, 1984). Metabolic rate underlies all biological processes through the allocation of energy to survival, growth, and reproduction, yet the total amount of energy an organism requires for these processes increases non-linearly with body mass (Gillooly et al., 2001). The rate of oxygen consumption (M_{O_2}), used as a proxy for metabolic rate, follows a power law relationship with body mass in which $M_{O_2} = aM^b$, where a is the species-specific coefficient or intercept, M is body mass, and b is the scaling exponent or slope of the relationship between metabolic rate and body mass. Within metabolic scaling theory, it has been argued that this scaling exponent falls near 0.75 for interspecific analyses of metabolic rate (Gillooly et al., 2001; Kleiber, 1932; Savage et al., 2004). Specifically, this refers to analyses using mean estimates of metabolic rate at a mean body mass, in contrast to intraspecific analyses where metabolic rate is estimated across a body size range within one species. However, as metabolic rate estimates are made for more and more species, the value of this scaling exponent is becoming increasingly scrutinised (Glazier, 2005, 2010; White et al., 2006). There are many inter- and intraspecific examples where the scaling exponent varies greatly across taxa – indeed, the exponent appears to be closer to 0.89 in fishes (Jerde et al., 2019) – yet the physiological and ecological factors underlying this variation are still poorly understood (Bokma, 2004; Killen et al., 2016; Norin and Gamperl, 2017).

Gill surface area (gill area) follows a similar power-law relationship with body mass (Gillooly et al., 2016; Hughes, 1984; Nilsson and Östlund-Nilsson, 2008) and is hypothesized to be a key factor in the scaling of metabolic rate in aquatic ectotherms, such as fishes (De Jager and Dekkers, 1975; Hughes, 1972; Hughes, 1984). Importantly, oxygen supply is increasingly viewed to limit performance and metabolic rate in this group, particularly at higher temperatures (Pörtner and Knust, 2007; Rubalcaba et al., 2020). Recently, renewed attention has been paid to the gill oxygen limitation theory, which suggests that gill area (a two-dimensional surface area) cannot increase isometrically with body mass (a three-dimensional volume) and may limit the uptake of oxygen and other resources into a fish's body, thus limiting the fuel available

for metabolism and constraining metabolic rate to a hypoallometric slope (<1) (Pauly, 2010; Pauly, 2021; Pauly and Cheung, 2017). This hypothesis gained scrutiny when Cheung et al. (2013) applied this theory to suggest that the maximum size a fish can reach will be reduced under climate change, where the increase in metabolic demand under warmer environmental temperatures will not be sufficiently met by a fishes' gill area, thus limiting maximum size. This theory is primarily based on the hypothesis that gill area (oxygen supply) and metabolic rate (oxygen demand) are matched, such that metabolic rate is constrained by the amount of gill area available for gas exchange (Pauly, 2010; Pauly, 2021). It assumes that gill area cannot scale with body mass with a slope at or above one due to limitations on the scaling of the gill components, specifically lamellar surface area, lamellar frequency, and filament length, where a fish's head will eventually "run out of space" for more gill tissue (Pauly and Cheung, 2017). However, this is in direct contradiction to widely accepted physiological view that causality flows the other way and gill area is adapted to match metabolic demand (Lefevre et al., 2017). While gills are indeed a surface, that surface is highly folded to increase the area available for exchange, potentially at a much greater rate than what is predicted for gill growth isometric to body volume (surface area/volume = 0.67) (Lefevre et al., 2017; Wegner, 2016). At the same time, the gills are also the main exchange surface for waste products and ion regulation between the fish and its surrounding environment (Evans et al., 2005; Wegner, 2016). Ion regulation is metabolically costly and likely underlies selection against "excess" gill area (Ern et al., 2014). The interspecific evidence for the limitation proposed by the gill oxygen limitation theory depends on estimates of metabolic rate and gill area made separately for individuals of different, unmatched body sizes (Gillooly et al., 2016; Lefevre et al., 2017). There are few studies which estimate both gill area and metabolic rate within the same species and which use a sufficiently wide body size range to produce reliable allometric regression coefficients (De Jager and Dekkers, 1975). Even less work estimates both gill area and metabolic rate in the same individual animals, removing the confounding factor of individual variation and providing a direct test of the relationship between these two traits (Li et al., 2018; Luo et al., 2020).

While it is accepted that the allometric scaling of gill area is related to that of metabolic rate, the underlying factors governing this relationship are still poorly understood (De Jager and Dekkers, 1975). Gill area should be large enough to supply a

fish with sufficient oxygen to fuel activity above resting metabolic rate (RMR) in order to allow the animal to carry out activities to ensure survival, growth, and reproduction (Hughes, 1984; Wegner, 2016). In most cases, it is hypothesized that gill area should scale closer to the scaling exponent for maximum metabolic rate (MMR) and body mass, as MMR would incorporate active metabolic levels needed to carryout energetically expensive activities such as active foraging and escaping predators (Bishop, 1999; Glazier, 2005; Hughes, 1984). However, most of the support for this hypothesis comes from work done in relatively active tuna and salmonid species, where RMR, MMR and gill area were each estimated in separate animals (Graham and Laurs, 1982; Hughes, 1984; Muir and Hughes, 1969). In contrast, a study using six carp species showed that the slope of gill area was not significantly different from RMR in five of the six tested species (Luo et al., 2020). Further, there are currently no studies which estimate gill area, RMR and MMR together in the same individuals for a direct comparison, making it difficult to tell whether a difference in scaling exponents between gill area and RMR is related to the scaling exponent of MMR.

Within and across species, MMR often scales with body mass with a steeper slope than RMR and body mass (Brett and Glass, 1973; Killen et al., 2007; Savage et al., 2004). Examining the allometry of MMR relative to RMR provides insight into a species' aerobic scope, or capacity for energy expenditure above rest, which may be an indicator of an organism's ability to respond to environmental extremes (Deutch et al., 2015; Pörtner and Knust, 2007). The underlying physiological mechanism for this divergence in scaling exponents is unknown, but activity level and hence, oxygen demand, is thought to play a role. The metabolic level boundaries hypothesis suggests that the contrasting effects of (1) surface area to volume constraints and (2) volume limits on resting tissue maintenance costs and power production act to produce steeper metabolic rate scaling exponents during periods of strenuous activity (Glazier, 2005, 2009). Here, metabolic level specifically refers to the elevation of the scaling relationship between metabolic rate and body mass (Killen et al., 2010; Glazier 2005). This hypothesis can also be used to explain some of the variation in intraspecific metabolic scaling exponents seen across species. Here, relatively inactive species with lower oxygen demands are hypothesized to be less limited by surface area to volume constrains on oxygen and resource exchange, and thus have metabolic scaling exponents nearly proportional to body mass and significantly steeper than those of more

active species (Glazier, 2005; Killen et al., 2010). This leads to the hypothesis that the allometric scaling of gill area may also be related to a species' lifestyle, where inactive species may have scaling exponents at or close to 1, with more active species having shallower exponents. Thus, in a relatively inactive benthic fish species, we may expect the allometric slope of gill area to fall nearer to the slope of RMR than to MMR and to see relatively steep slopes for all traits.

Here, we examined the allometric relationship between oxygen supply and demand using paired estimates of resting and maximum metabolic rate and gill area in 19 individual California Horn Shark (*Heterodontus francisci*, Girard 1855), using a wide body size range representing the full ontogeny of the species. We asked three questions; (1) does the allometric slope of MMR fall above that of RMR, and (2) is the allometric slope of GSA closer to that of MMR than to RMR? To determine how California Horn Shark increase their gill area as they grow in size, we also examined the allometric scaling of each gill area component (lamellar surface area, lamellar frequency, and filament length) and compared each estimate to the values expected under surface-area-to-volume constraints.

2.3. Methods

First, we collected 19 California Horn Shark individuals and acclimated them to the lab aquaria for a minimum of two weeks. Second, for each individual, we estimated resting metabolic rate (RMR) using intermittent flow respirometry, after which we estimated maximum metabolic rate (MMR) using a chase-to-exhaustion protocol. Third, after estimating metabolic rate, we sacrificed each individual and estimated its gill area. Finally, we compared the allometric scaling of each metabolic trait (gill area, RMR and MMR) on a $\log_{10}$–$\log_{10}$ scale.

2.3.1. Animal acquisition and husbandry

California Horn Shark ranging in size from 0.039–4.44 kg (n = 19) were caught between June and October 2019 as bycatch during overnight gillnet surveys or by hand using SCUBA in Mission Bay in San Diego, CA and off Scripps Pier in La Jolla, CA. Upon capture, individuals were transported to the Southwest Fisheries Science Center (SWFSC) Experimental Aquarium in aerated coolers with frequent water changes to

maintain oxygen saturation and reduce waste build up. Individuals were allowed to acclimate to captivity until they resumed regular feeding and for at least two weeks before experimentation. Sharks were held in 300 × 150 × 90 cm oval tanks (~3,200 L) continuously fed with fresh filtered and UV sterilized seawater (18 ± 0.5°C, ≥100% oxygen saturation, 33.5‰, salinity). This temperature was chosen as it falls at the middle of the species' natural range and was within about 1°C of the ocean temperature at which individuals were collected. For identification, a photograph was taken of the dorsal fin spot pattern on each individual upon arrival. Individuals were fed to satiation every 3-5 days using human-grade market squid (*Doryteuthis opalescens*) and mackerel (*Scomber japonicus*) and were fasted for a minimum of 48 hours before experiments to remove the influence of specific dynamic action on metabolic rate estimates. The two smallest individuals tested (one male and one female, 0.0387 kg and 0.0590 kg, respectively) were derived from eggs laid by an adult female collected with other individuals but not used in respirometry experiments. Once hatched, these small sharks were fed shucked bean clams (*Donax gouldii*) and squid tentacles daily until deemed strong enough to be fasted and exercised (10+ weeks post hatch). All shark husbandry and experimentation were conducted under protocol #SW1801 of the SWFSC Animal Care and Use Committee.

2.3.2. Respirometers and experimental setup

The rate of oxygen consumption over time (M_{O_2}) was measured for each individual using respirometers consisting of a holding chamber proportional to the size of the shark and a short recirculation loop containing a fiber optic oxygen sensor and temperature probe connected to either a Fibox 3 or Fibox 4 oxygen meter (Presens, Regensburg, Germany) (Clark et al., 2013; Svendsen et al., 2016). Seven separate respirometer chambers of increasing width and length were used to accommodate the wide size range of individuals used in this study. The six larger chambers were commercial acrylic cylinders and varied in size from 5.825 L to 52.5 L (Loligo Systems, Denmark). The smallest chamber (2.58 L) was constructed onsite from a 28.1 x 19.3 x 7.9 cm rectangular Tupperware outfitted like the cylindrical chambers to accommodate the two small juvenile sharks. Chamber-to-fish volume ratio varied from 11.8:1 to 66.4:1. During trials, the respirometer was placed in a large water bath to maintain a consistent experimental temperature (18 ± 0.5°C) and to allow the system to be flushed with

aerated seawater between oxygen depletion measurements through inlet / outlet valves on opposing ends of the chamber. Water entering the chamber from both the recirculating and inlet valve was forced against a splitter or a wide plate to aid in mixing within the chamber. To reduce bacterial growth, water baths were constantly supplied with fresh, UV sterilized aerated seawater (18 ± 0.5°C, salinity 33.5‰, oxygen ≥ 100%) at a rate to fully exchange the bath water every 30–60 min and systems were washed with detergent or sterilized with ethanol between experiments.

2.3.3. Estimation of resting metabolic rate

We estimated RMR for each individual using automated intermittent flow respirometry. One at a time, individuals were moved from their holding aquaria to individual respirometer chambers set up within the water bath. Black plastic sheets were draped over the chambers to prevent visual disturbance. When time and space allowed, two animals were run at the same time within the water bath but in individual respirometers separated by a black plastic divider so they could not see each other. Individuals were allowed to acclimate in the respirometer overnight for 12 hours before beginning oxygen consumption measurements, as California Horn Shark were found to be most calm during the first daylight hours of the morning (Chabot et al., 2016; Luongo and Lowe, 2018). California Horn Shark are nocturnal and relatively inactive, preferring to hide in rock crevices during the day to avoid predators, and thus showed little to no activity inside the respirometer while at rest (Meese and Lowe, 2020).

The automated intermittent flow respirometry protocol was made up of repeated cycles each consisting of a closed and flush period. The flush pump was turned off and the chamber was sealed for measurement of oxygen depletion during the closed period, then opened during the flush period to allow fresh, oxygenated seawater to be pumped into the chamber to fully exchange and oxygenate the water around the individual. Cycles began when the individual was placed in the respirometer chamber and were automated using timers to turn the flush pumps on and off. One-way check valves were fitted on the inflow and outflow valves to seal the chamber during the closed period. Because chamber sizes and shark body mass varied across individuals in our study, the amount of time used to fully flush each chamber with oxygenated seawater between closed periods also varied (5-10 minutes). Oxygen concentration within the chamber was measured once every 5 seconds.

Within the closed period, the rate of oxygen consumption over time (M_{O_2}) was determined using the equation

$$M_{O_2} = [(V_r - V_f) \times \beta_{O_2}] \ / M_f \quad (1)$$

where V_r is the respirometer chamber volume in litres, V_f is the fish volume (assumed to be equivalent to the fish mass, M_f), and β_{O_2} is the rate of oxygen consumption over time. For each closed period, the first three minutes were removed to allow for water mixing, then the following seven minutes were used to estimate M_{O_2}. Measurements occurring within the 12 hr acclimation period after the individual was first placed in the respirometer chamber were removed. Then, the mean of the lowest three M_{O_2} measurements occurring during the remaining five to nine hours the individual was in the chamber was used as the RMR estimate for that individual. Background respiration was measured in sealed clean respirometers and immediately following removal of the shark in RMR pilot experiments, when bacteria buildup would have been highest, and was deemed negligible (<3%) in all but the trial for the smallest individual (body mass 0.0391kg). For this individual, the level of background respiration during the trial was calculated assuming a linear increase over time from just before the individual was placed in the respirometer chamber to just after it was removed. Then, M_{O_2} for each measurement period was corrected by subtracting this calculated level of background respiration and RMR was estimated for this individual (Rodgers et al., 2016).

2.3.4. Estimation of maximum metabolic rate

Immediately following estimation of RMR for each individual, MMR was estimated using one of two methods: chase alone or chase with air exposure, herein termed "*chase*" and "*chase + air*", respectively. Following a two-day recovery period, the other MMR method was used on that individual. The order of MMR methods for each individual was randomly assigned. For either the *chase* or the *chase + air* methods, the protocol began by removing the individual from the respirometer chamber following RMR and placing it in a large circular chase tank filled with aerated seawater siphoned from the holding aquarium (18 ± 0.5°C). The individual was then exercised to exhaustion by grabbing and pinching at its tail and by turning it over with gloved hands. It was deemed exhausted once it stopped bursting away and began resting on the bottom of the chase

tank between stimuli (usually after 4-7 minutes of chasing). If undergoing the chase method, the individual was then immediately transferred to the respirometer chamber for measurement of post-exercise oxygen consumption, where oxygen concentration was recorded once every second until the oxygen concentration within the chamber reached 80% saturation (Reidy et al., 1995). Transfer time from the chase tank to start of oxygen depletion measurements was typically less than 30 s. In the *chase + air* method, the individual was placed in a holding bin without water for ten minutes with a wet cloth was draped over the eyes and gill slits before it was transferred to the respirometer. Due to their small size, the two MMR trials (*chase, chase + air*) for the two newly hatched individuals were separated by at least four days to allow the shark to fully recover and feed between trials.

MMR was estimated using a rolling regression model following methods outlined in Chapter 3, where the 2-min regression window corresponding to the highest rate of oxygen consumption within the oxygen depletion trace was used to calculate MMR using equation (1). A linear mixed-effects model with general linear hypothesis test showed that estimates produced with the MMR *chase* and MMR *chase + air* methods did not differ significantly and thus only the MMR *chase* results are shown and used in further analyses below (see Supplementary for MMR method analysis and MMR *chase* and MMR *chase + air* comparison).

2.3.5. Estimation of gill surface area

Once all respirometry trials were completed, the individual was sacrificed with an overdose of the anesthetic MS-222, patted dry and weighed. Its head was removed posterior to the last gill arch, and the entire head was then fixed in seawater buffered 10% formalin for a minimum of two weeks for tissue fixation before beginning gill dissections.

Gill surface area for each shark was estimated as

$$A = L_{fil} \times 2n_{lam} \times A_{lam} \quad (2)$$

where L_{fil} is the total length of all gill filaments on both sides of the head, n_{lam} is the lamellar frequency (i.e., the mean number of lamellae per unit length on one side of a filament, multiplied by two to account for lamellae on both sides of the filament), and A_{lam}

is the mean bilateral surface area of a lamellae (Bigman et al., 2018; Wegner, 2011; Wegner et al., 2010). To accomplish this, all five gill arches were removed from the right side of the head and all filaments on all nine hemibranchs were counted and evenly divided into eight bins per hemibranch. A magnified photo was taken of the median filament in each bin, which was assumed to be representative of all filaments in that bin (Meiji Techno America EMZ-8TR microscope with Moticam 5+ camera, San Jose, USA). The length of this filament, including the section beneath the gill arch branchial canopy, was traced and measured using ImageJ imaging software (National Institutes of Health, USA, Java 1.8.0_172) (Wegner, 2016). The total length of all filaments on all hemibranchs on the right side of the head was calculated by multiplying the length of the median filament in each bin by the total number of filaments in that bin, then summing the length of all filaments in all bins. This length was doubled to account for the length of filaments on the left side of the head which were not measured. Following this, the median filament from each bin on the posterior hemibranch on the second gill arch was removed for lamellar measurements. Each excised filament was turned on its side to show the lamellae and a magnified photo was taken at each of the tip, middle and base sections for estimation of lamellar frequency (number of lamellae per mm) using ImageJ software. A cross section was then made at each of these three locations on the filament, which was then turned on its side to take a magnified photograph of the extended lamellae on both sides of the filament. Lamellar surface area in mm^2 was estimated using ImageJ software by tracing the outline of the lamella on one side of the filament, then doubling it to represent the bilateral surface area of the lamella. Lamellar frequency (mm^{-1}) was estimated by averaging lamellar frequency measurements taken at each of the base, middle and tip of each individual filament, multiplying this mean by the total length of all filaments in that bin to give the total number of lamellae per bin, summing the total number of lamellae in all bins, then dividing this by the total length of all filaments on the hemibranch. Average lamellar surface area (mm^2) was estimated by taking the mean of lamellar surface area measurements taken at the same three locations as lamellar frequency on each filament, multiplying this mean by the total number of lamellae in that bin to give a total lamellar area per bin, summing the total lamellar area for all bins, then dividing by the total number of lamellae on the hemibranch. Lamellar frequency and surface area were measured on all median filaments from all nine hemibranchs on the first dissected individual. These measurements showed that the posterior hemibranch on the second gill arch was most

representative of the gills as a whole and thus lamellar frequency and mean lamellar surface area measurements from subsequent sharks were based solely on this hemibranch.

2.3.6. Statistical analysis

Using ordinary least-squares regression, we estimated the allometric slope of each of $\log_{10}$ gill area (cm^2), $\log_{10}$ RMR (mg O_2 h^{-1}), or $\log_{10}$ MMR (mg O_2 h^{-1}) as a function of $\log_{10}$ body mass (kg). When regressed as a function of body mass, gill area estimates for the two smallest sharks were highlighted as potential outliers and the model appeared to contain an inflection point. Using the `segmented` function from the package `segmented`, we fit a broken-stick regression with $\log_{10}$ gill area, $\log_{10}$ RMR, or $\log_{10}$ MMR as a function of $\log_{10}$ body mass to detect any potential inflection points in these relationships and estimate regression coefficients for each segment (Muggeo, 2003; 2008). We also plotted the ratio of gill area over metabolic rate, calculated as total gill area (cm^2) divided by either absolute RMR or MMR (mg O_2 h^{-1}) for each individual and $\log_{10}$ transformed, against $\log_{10}$ body mass. This ratio can be thought of as an estimate of the amount of gill area the individual possesses for each unit of metabolic rate (either RMR or MMR), or the amount of gill area an individual possesses after controlling for metabolic rate (not to be confused with a measure of the amount of gill area left over after metabolic is accounted for, or the amount of gill being used per unit of metabolic rate, as we cannot measure this). We then fit a broken-stick regression model to these data to examine how this ratio changed across the size range. Absolute aerobic scope was estimated as MMR-RMR (Norin and Gamperl, 2017). Factorial aerobic scope was calculated as the ratio of MMR to RMR from the power law functions of MMR and RMR (Killen et al. 2007).

We tested for a difference between the allometric slopes of RMR and MMR by fitting a linear mixed-effects model, where $\log_{10}$ metabolic rate estimate was set as a function of $\log_{10}$ body mass with metabolic rate type as an interaction term and individual as a random effect. Residuals were evenly distributed within each metabolic rate type (Shapiro-wilk test, $P > 0.05$), and homogenously distributed across models (Levene's test, $P > 0.05$). We then used the `emtrends` function from the package `emmeans` to compare slope estimates from our linear mixed-effects model (Lenth et al., 2020). This

analysis is similar to a basic ANCOVA but accounts for the influence of the random effect of individual in our model.

Finally, we examined the allometric slopes of each gill area component to understand how California Horn Shark increase their gill area as they grow. Using ordinary least-squares regression, we examined the scaling of each gill area component and plotted each of $\log_{10}$ total filament length (cm), $\log_{10}$ average lamellar frequency (mm^{-1}), and $\log_{10}$ mean bilateral lamellar surface area (mm^2) as a function of $\log_{10}$ body mass. Similar to gill area, there appeared to be a non-linear relationship between $\log_{10}$ lamellar surface area and $\log_{10}$ body mass, and we fit a broken stick regression to these data using the `segmented` function from the package `segmented` to test for any potential inflection points (Muggeo, 2003; 2008).

2.4. Results

When the allometric scaling of gill area was examined using a broken-stick regression, this model estimated an inflection point near the third smallest individual (0.203 kg body mass) and produced slope estimates of 0.540 ± 0.218 and 1.014 ± 0.151 for the regression segments corresponding to smaller and larger body mass individuals, respectively (Fig. 2-1a). When modeled using ordinary least squares regression, gill area scaled with body mass with a slope of 0.888 ± 0.077 (95% CI) across the full sample size of California Horn Shark (Fig. 2-1a). Comparing each model using AIC revealed that the broken-stick regression model was a better fit to the gill area data relative to the ordinary least-squares regression (Table 2-1).

The slope of MMR and body mass was hyperallometric (i.e. >1; 1.079 ± 0.044) and significantly steeper than the slope of RMR and body mass (0.971 ± 0.064) (P = 0.0036) (Figs. 2-1b, 2-2). For both RMR and MMR, the ordinary least-squares regression model was a better fit to the data than the broken-stick regression model when compared with AIC.

When we examined the ratio of gill area to metabolic rate across body mass on a $\log_{10}$–$\log_{10}$ scale, we found there was more gill area (cm^2) per unit metabolic rate (either RMR or MMR, mg O_2 h^{-1}) at the smallest relative to the largest body masses (Fig. 2-3). For example, according to the broken stick regression model, the mean ratio of gill area

to MMR would be 33% larger for the smallest individual relative to the gill area of the largest individual. The ratio of gill area to metabolic rate initially scaled with body mass with a negative slope for both RMR and MMR for the first regression segment, and similar to the broken-stick regression for gill area as a function of body mass (Fig. 2-1a), and inflection point was estimated near the third smallest individual (Fig. 2-3). Over the second regression segment covering the remaining larger individuals, the ratio of gill area to RMR increases slightly and the ratio of gill area to MMR decreases slightly.

Absolute aerobic scope (calculated as whole-organism MMR-RMR, then $\log_{10}$ transformed for analysis) increased with body mass with a slope of 1.101 ± 0.053 (Fig. 2-3a). Factorial aerobic scope (calculated as the ratio of MMR to RMR from the regression slopes) also increased with body mass, where factorial aerobic scope was 60% higher for the largest individual relative to the smallest individual (Fig. 2-3b).

The allometric slopes for the gill components of total filament length (cm), average lamellar frequency (mm^{-1}), and mean bilateral lamellar surface area (mm^2) were 0.404 ± 0.019 (95% CI), -0.101 ± 0.013, and 0.581 ± 0.0850, respectively (Fig. 2-5). When the broken-stick and ordinary least-squares regression models were compared with AIC, the broken-stick regression model for lamellar surface area was deemed a better fit (Table 2-1). This model estimated an inflection point at the third smallest individual and the slope estimates for the lower- and upper-line segment were 0.054 ± 1.162 and 0.741 ± 0.091, respectively.

Model	AIC	Log-likelihood	r^2	df
Gill area broken-stick regression	-40.4	25.2	0.985	5
Gill area OLS regression	-32.8	19.4	0.972	3
RMR broken-stick regression	-39.6	24.8	0.987	5
RMR OLS regression	-39.6	22.8	0.984	3
MMR broken-stick regression	-55.1	32.6	0.995	5
MMR OLS regression	-53.9	30.0	0.994	3
Lamellar area broken-stick regression	-42.8	26.4	0.971	5
Lamellar area OLS regression	-28.9	17.5	0.92	3
Filament length broken-stick regression	-89.1	49.6	0.994	5
Filament length OLS regression	-85.5	45.8	0.992	3
Lamellar frequency broken-stick regression	-97.0	53.5	0.943	5
Lamellar frequency OLS regression	-100.2	53.1	0.94	3

Table 2-1 **Results of the comparison between broken-stick and ordinary least-squares (OLS) regression models for each tested trait. For both gill area and lamellar area, AIC indicated that the broken-stick regression model was a better fit relative to the ordinary least-squares regression model. In all other cases, there was no significant difference in model fit between the compared models and ordinary least-squares regression was taken as the best fit model.**

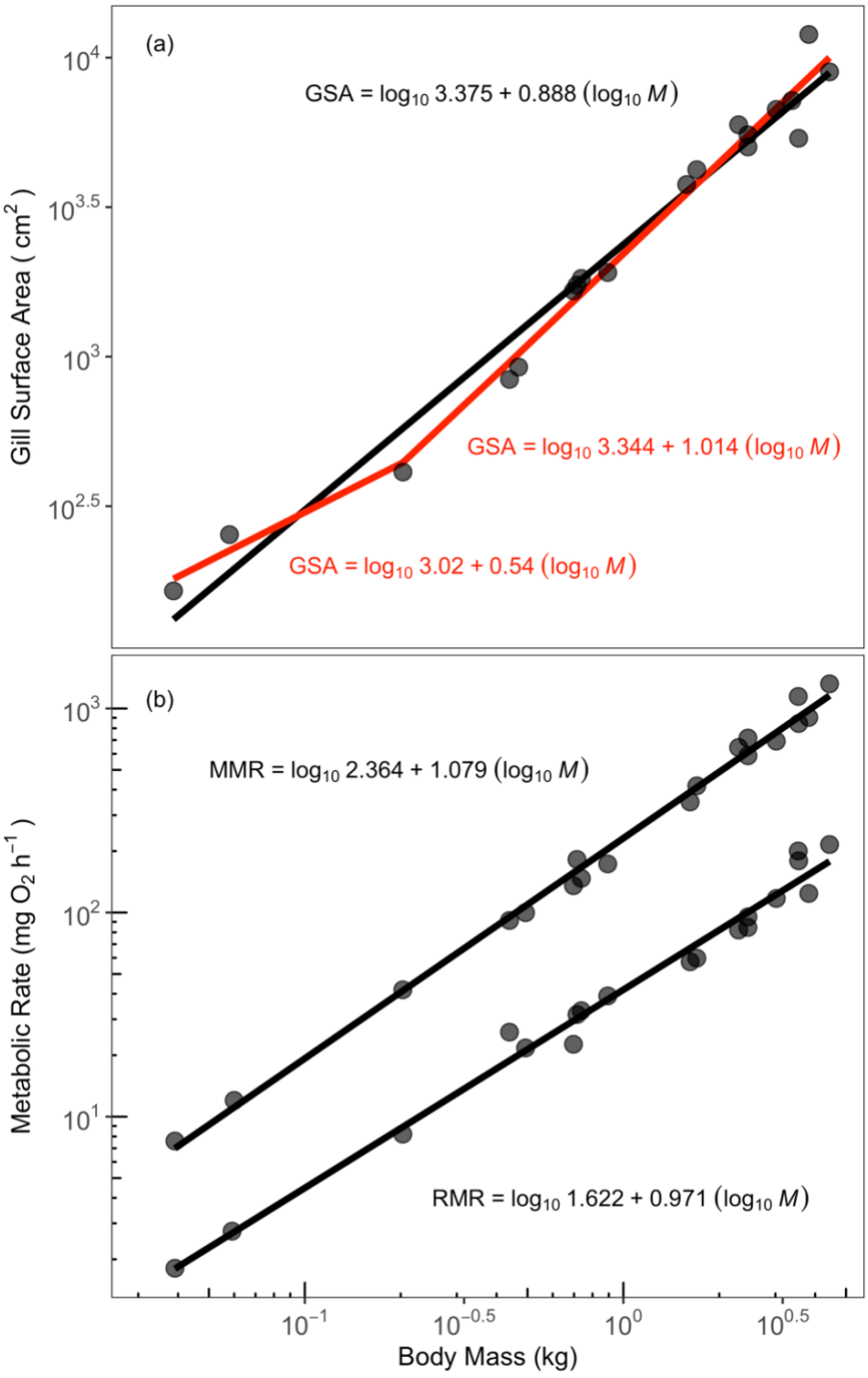

Figure 2-1 **Allometric scaling of (a) gill area (GSA), (b) maximum metabolic rate (MMR), and resting metabolic rate (RMR) as a function of body mass on a $\log_{10}$–$\log_{10}$ scale, represented by the black regression lines. (a) The gill area broken-stick regression is plotted in red, with the equation for each regression segment placed nearest to the segment it represents.**

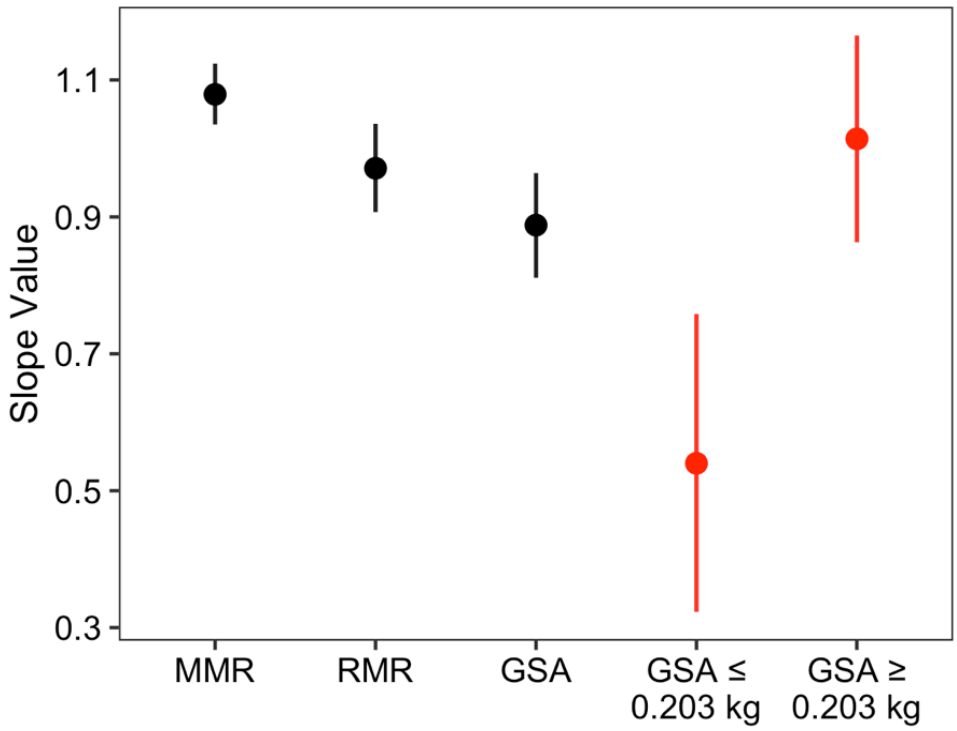

Figure 2-2 **Slope estimates for each of maximum metabolic rate (MMR), resting metabolic rate (RMR), and gill area (GSA), ± 95% confidence intervals. The gill area slope estimates for each line segment estimated with the broken-stick regression model are indicated in red.**

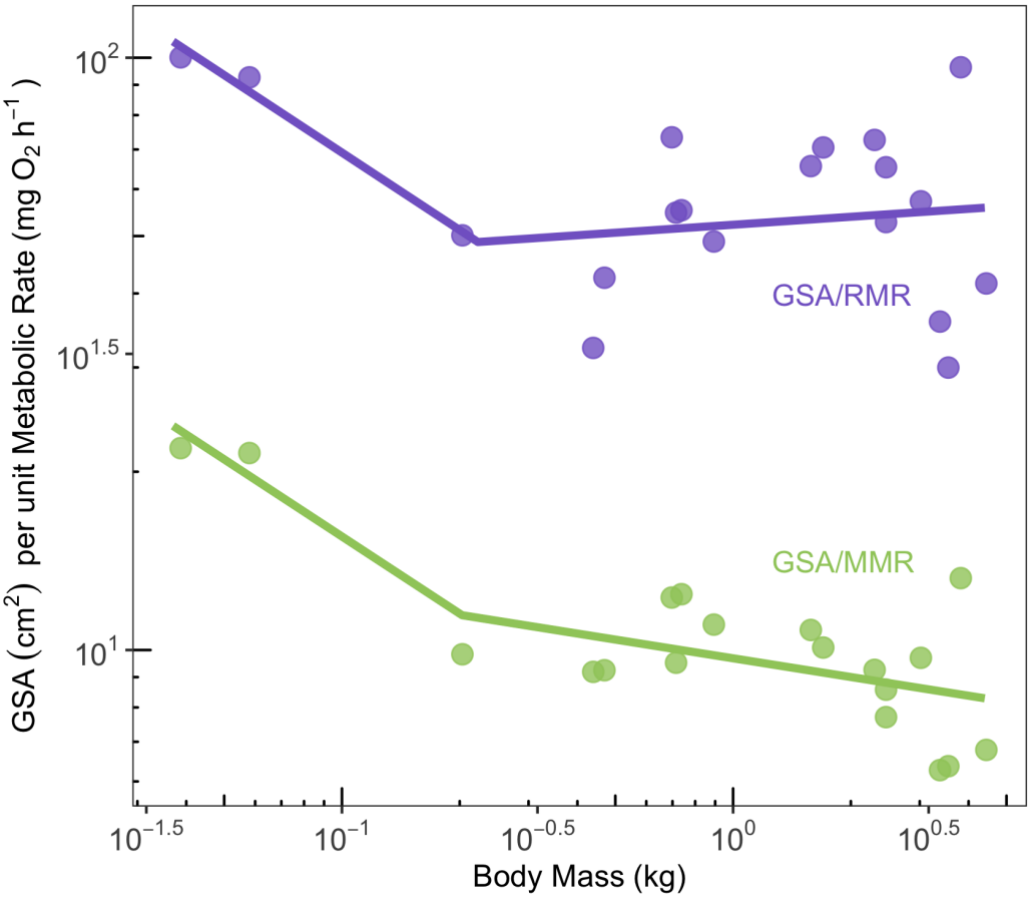

Figure 2-3 **The allometric relationship of the ratio of gill area (GSA) to metabolic rate for each of resting (RMR, purple) and maximum (MMR, green) metabolic rates on a log_{10}–log_{10} scale. Specifically, total measured gill area (cm^2) divided by absolute metabolic rate (mg O_2 h^{-1}) for each individual. Each point represents the amount of gill area that individual possesses relative to one unit of metabolic rate at that individual's body mass. Because RMR requires less oxygen than MMR, there is a larger ratio of gill area per unit metabolic rate, and thus the ratio of GSA/RMR is higher than the ratio of GSA/MMR. Fitting a broken-stick regression to these data helps us see how the ratio of gill area to metabolic rate may change with body mass – the two smallest sharks appear to have relatively more gill area per unit metabolic rate when compared to the remaining sharks, and the slope (or rate of change) of this ratio becomes shallower at the third smallest individual. This coincides with what we observed when gill area was regressed as a function of body mass and anlyzed with a broken-stick regression model (Fig. 2-1a).**

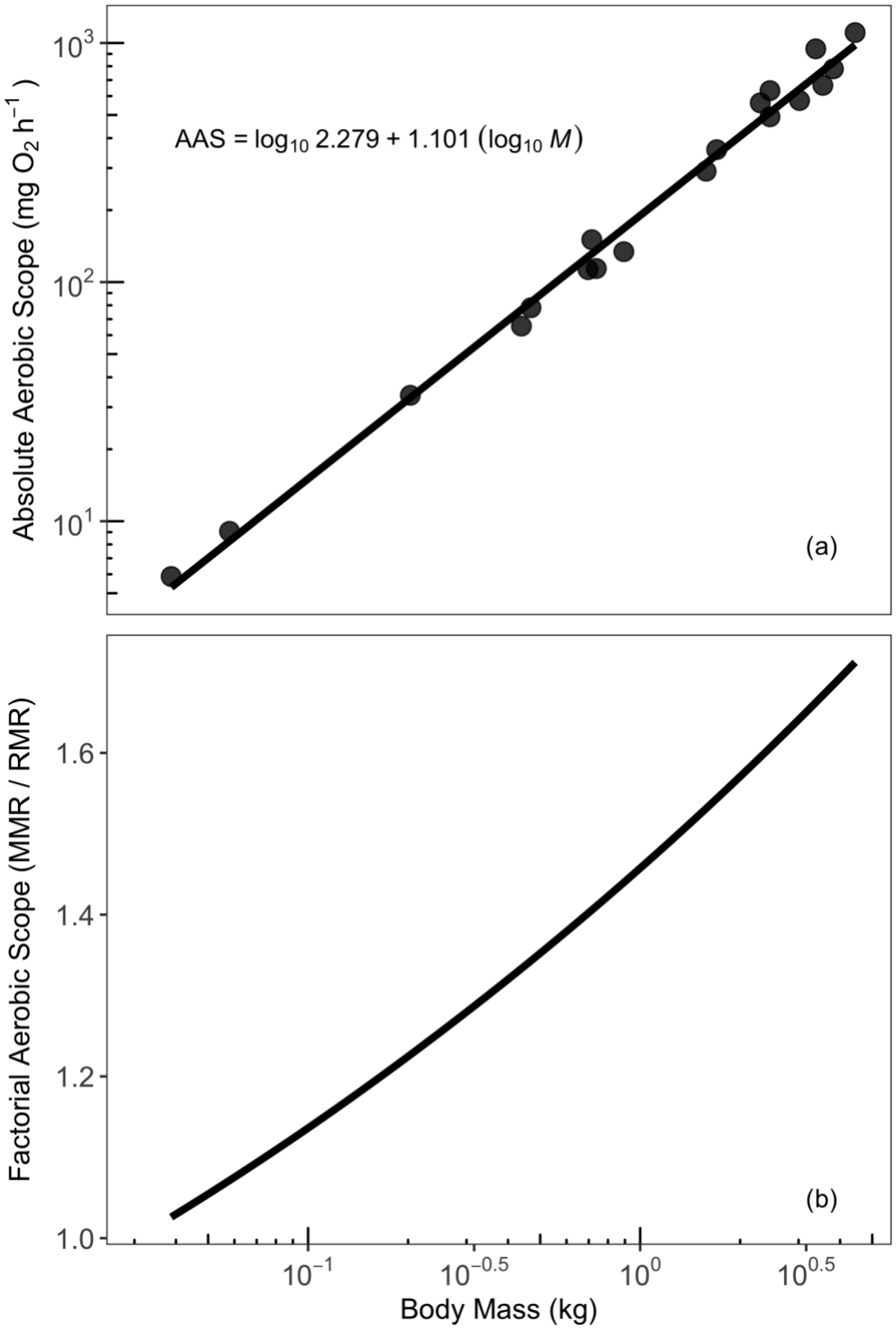

Figure 2-4 **(a) Absolute aerobic scope (AAS), calculated as MMR-RMR, and (b) factorial aerobic scope, calculated as the ratio of MMR to RMR from the respective power law functions. In each analysis, aerobic scope increased with body mass.**

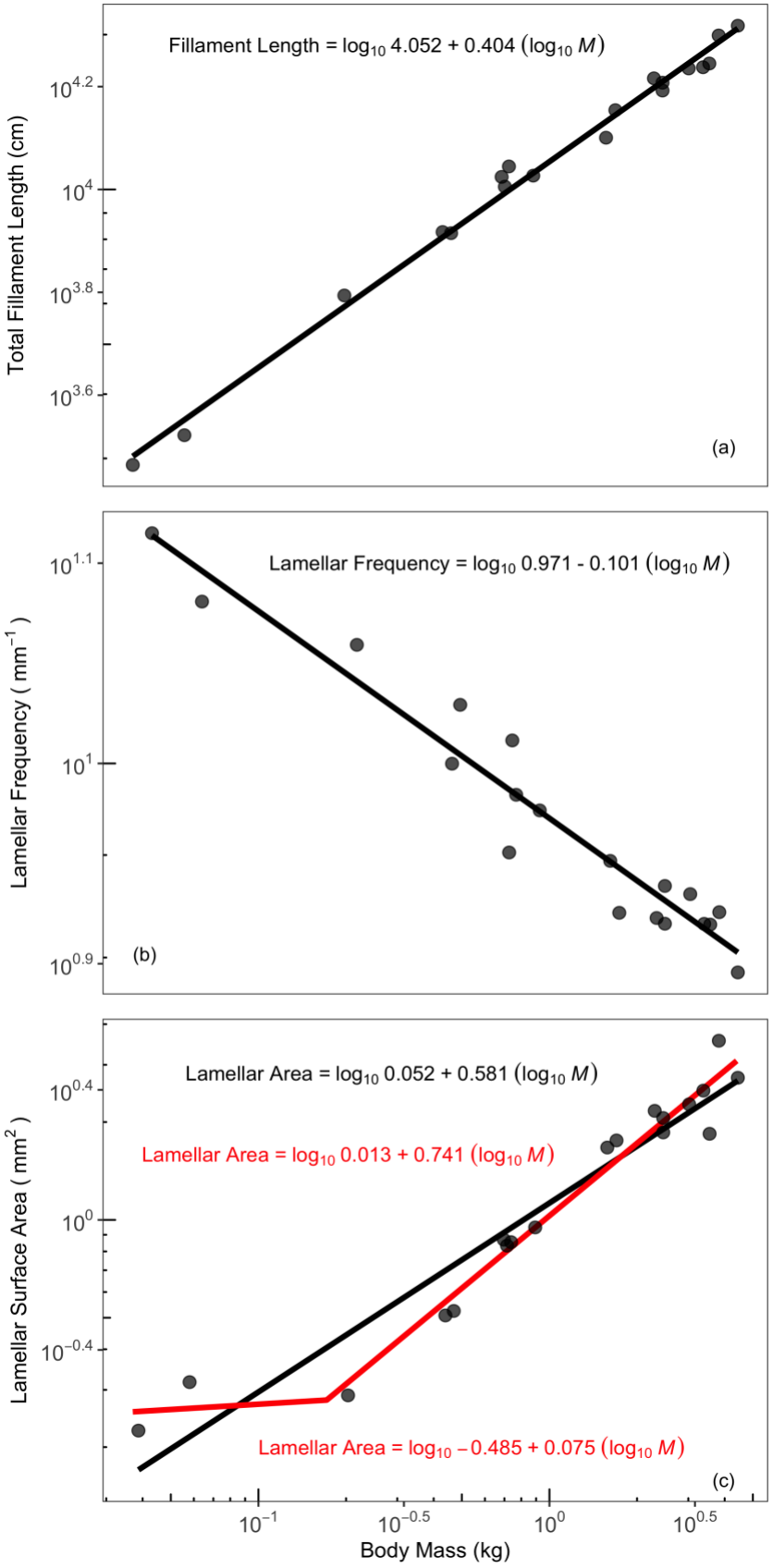
Fillament Length = log10 4.052 + 0.404 (log10 M)
Total Fillament Length (cm)
10^4.2
10^4
10^3.8
10^3.6
(a)
Lamellar Frequency = log10 0.971 - 0.101 (log10 M)
Lamellar Frequency (mm^-1)
10^1.1
10^1
10^0.9
(b)
Lamellar Area = log10 0.052 + 0.581 (log10 M)
Lamellar Area = log10 0.013 + 0.741 (log10 M)
Lamellar Area = log10 −0.485 + 0.075 (log10 M)
Lamellar Surface Area (mm^2)
10^0.4
10^0
10^−0.4
(c)
10^−1
10^−0.5
10^0
10^0.5
Body Mass (kg)

Figure 2-5 **The relationship between each of (a) total filament length (cm), (b) average lamellar frequency (mm^{-1}), or (c) mean bilateral lamellar surface area (mm^2) and body mass (kg) for 19 California Horn Shark, represented by the black regression lines. (c) The broken stick regression model for lamellar surface area is plotted in red, with the upper and lower segment equations nearest to the segment they represent. The expected scaling exponents for each gill area component, based on isometric growth (2/3 the rate of body mass), are 0.33, -0.33, and 0.67 from (a) to (c), respectively.**

2.5. Discussion

Our results showed that in California Horn Shark, an inactive, small-bodied shark, oxygen demand and supply are closely matched and a two-dimensional gill area can increase at the same rate as the three-dimensional mass of this organism. When viewed across our full sample size representing a nearly complete body size range, the slopes of RMR and MMR were isometric (~1) and hyperallometric (>1), respectively (Fig. 2-1b), and, surprisingly, we found that the relationship between gill area and body mass was best explained by a broken-stick regression model relative to an ordinary least-squared regression model (Fig. 2-1a). Additionally, the slope of MMR and body mass was significantly steeper than the slope of RMR and body mass and aerobic scope increased with body mass (Figs. 2-1b, 2-2, 2-4). Here, we first discuss the allometric scaling of metabolic rate and compare the slope of MMR to RMR. Second, we compare the scaling of metabolic rate to the scaling of gill area. Third, we discuss how our findings fit into the larger framework of metabolic scaling in the context of oxygen supply and demand. Finally, we discuss the potential physiological underpinnings of the allometric scaling of gill area.

Across a body size range representing the near-complete ontogeny of California Horn Shark, our results showed that the allometric slopes of RMR ad MMR were isometric and hyperallometric at 0.971 ± 0.064 and 1.079 ± 0.044, respectively (Fig. 2-1b, 2-2). This pattern is consistent with the metabolic level boundaries hypothesis, which predicts that relatively inactive species are not constrained by surface area limitations on oxygen and resource supply and exhibit metabolic rate slopes nearer to isometry (Glazier, 2005; Killen et al., 2010). In contrast, more active species may be more limited by surface areas, such as the gills, and exhibit relatively shallow metabolic rate exponents (Glazier, 2005; Killen et al., 2010). Killen et al. (2010) show this activity-scaling pattern holds across 89 fish species binned into either four ecological lifestyle categories (pelagic, benthopelagic, benthic, and bathyal) or four swimming modes (thunniform, carangiform, subcarangiform, and anguilliform), and suggested these factors may be partly responsible for the variation in intraspecific scaling exponents observed across species. However, this ecological lifestyle measure of activity is conflated with phylogeny. Additionally, the metabolic level boundaries hypothesis may underly another of our key findings – metabolic level had a significant effect on slope

estimate whereby the slope of MMR was significantly steeper than the slope of RMR (Glazier, 2005, 2009). Here, metabolic rate during strenuous exercise should be influenced primarily by the volume-related scaling of power production (which scales with muscle volume), yielding an allometric slope nearer to one, while lower, more sustainable metabolic rates should be more closely tied to surface area to volume constraints and scale with a shallower exponent (Glazier, 2005; Glazier, 2009). While our results match those predicted by this hypothesis, our work does not speak to the directionality of the relationship between metabolic rate and surface area (gill area or otherwise). Additionally, there are cases where the prediction of steeper scaling of MMR above RMR does not hold. For example, in fishes of the family Cyprinidea, an opposite pattern has been found where the slope of RMR and body mass was steeper than or similar to the slope of MMR and body mass (Luo et al., 2015; Zhang et al., 2014). More paired ontogenetic examples in species from a wider range of activity levels are needed to help us better understand the interplay of oxygen uptake, demand, and activity level.

We found that the allometric slope of gill area was best represented by a broken-stick regression model, suggesting a mis-match may exist between gill area and metabolic rate for juvenile California Horn Shark relative to adolescents and adults (Fig. 2-1a, Table 2-1). The inflection point in the gill area-body mass relationship suggests a steepening of slope near 30 cm total length (Fig. 2-1a), corresponding to the size at which California Horn Shark are thought to transition from their juvenile to adolescent life stage (35 cm) (Ebert et al., 2013). This inflection point is not seen in either the MMR nor RMR regressions, suggesting that there may be a disconnect between metabolic demand and supply at this early developmental stage (Fig. 2-1b, Table 2-1). There are other examples where the allometric scaling of gill area may change with body mass; in larval teleost fishes, hyperallometric scaling of gill area occurs post-hatch to compensate for the simultaneous reduction in cutaneous gas exchange (Pauly and Cheung, 2017; Post and Lee, 1996). In contrast to teleosts, elasmobranchs may not have the same opportunity to respire through their skin. They emerge from their egg cases resembling adults, covered in calcareous dermal denticles, and mainly respire across their gill tissue (Rodda and Seymour, 2008; Toulmond, 1982). Because of this, at least at later stages of development within the egg case, they must rely on their gills as the sole gas exchange surface, possibly resulting in a relatively large gill area as an adaptation to protect against potential hypoxia in their surrounding environment or within the potentially

diffusion-limited egg case itself (Di Santo et al., 2016). Further, embryonic metabolic rates may be particularly high in the embryos of egg-laying elasmobranchs because of the need for highly active tail beating to ventilate the egg capsule and circulate water (Leonard et al. 1999). This means that once hatched, they may possess excess gill area relative to their oxygen demand, similar to the pattern seen in California Horn Shark (Fig. 2-3). As they increase in body size into adolescence, the ratio of gill area to metabolic rate may decrease, perhaps until gill area is again matched to metabolic needs and from which point it scales similarly to metabolic rate (Figs. 2-1, 2-3). In juveniles, gill area first increases at a slower rate relative to both RMR and MMR (0.540 ± 0.218), possibly as gill area is shifted to match the needs of a new free-swimming life stage (Figs. 2-1, 2-3). Then, in adolescents and adults, the allometric slope of gill area falls between that of RMR and MMR (1.014 ± 0.151, 0.971 ± 0.064, and 1.079 ± 0.044, respectively) (Fig. 2-2). Examining the amount of gill area per unit metabolic rate (cm^2 gill area for each mg O_2 h^{-1} metabolic rate) highlights how this pattern may lead to a change in oxygen supply capacity with body mass in California Horn Shark (Fig. 2-3). The gills for the two smallest sharks appear 'overbuilt' for their metabolic needs, where the mean ratio of gill area to MMR is estimated to be 33% larger for the smallest individual relative to the largest. This is a key area for further research – in contrast to our results here, previous evidence has shown there to be a relatively low ratio of gill area to metabolic rate in newly hatched bony fishes, and future work should test if our findings for California Horn Shark apply across more egg-laying elasmobranchs (Pauly and Cheung, 2017; Post and Lee, 1996).

Previous work has suggested that the allometric slope of gill area should fall closer to the allometric slope of MMR in order to supply the fish with sufficient oxygen for activity above rest (Hughes, 1972; 1984). This makes sense when we consider that the allometric slope of MMR is often steeper than that of RMR and that the animal may need sufficient gill area to meet this higher relative oxygen demand (Bishop, 1999; Hughes, 1984; Killen et al., 2007). California Horn Shark are inactive and nocturnal, with one study showing that females and males spend most (88.1–93.3%) of their day at rest in shelters and only actively hunt for about 50% of the night (Meese and Lowe, 2020). Thus, they may not often require the gill area necessary for relatively high levels of energy expenditure, and hence their gill area scales with body mass with a slope not significantly different from either RMR or MMR. In contrast, a relatively active species (e.g. Rainbow Trout *Salmo salar*) would more often require high levels of oxygen to fuel

its active lifestyle and may display a slope of gill area and body mass nearer to the slope of MMR and body mass (Hughes 1984). However, there is evidence that the allometric slope of gill area may not correlate well with a species' lifestyle. Bigman et al. (2018) show that the intercept, but not the slope, of gill area and body mass was related to habitat type and caudal fin aspect ratio (a measure of activity level) in twelve elasmobranch species. This highlights the need for further work in a wider diversity of species testing the interplay of body size, activity level and temperature to understand the allometric scaling of gill area and oxygen limitation (Rubalcaba et al., 2020).

One hypothesis proposed to explain the patterns of gill surface area scaling we see across fishes, the gill oxygen limitation theory, states that geometrical constraints prevent adult fish from growing gills in proportion to their body mass, i.e., gills that scale isometrically with body mass (Pauly, 2010; Pauly, 2021; Pauly and Cheung, 2017). However, when gill area is analyzed using a broken-stick regression model, we find isometric scaling in California Horn Shark across a near full body size range. The widely held view is that gills are adapted to match metabolic needs, rather than that metabolism is constrained by a limited gill area (Lefevre et al., 2017). This lack of constraint may be especially true for California Horn Shark, which spend a considerable amount of time motionless or swimming slowly, as their gills may have more freedom to take up space in the head at the expense of hydrodynamics (Meese and Lowe, 2020). In the closely related Pork Jackson Shark (*Heterodontus portusjacksoni*), there is an increase in head length and width in proportion to total body length as the shark matures (Powter et al., 2010). This may offer an increase in space available for gills, reducing any possible morphological constraint to gill surface area that might be more of an issue for the hydrodynamically sleek and active shark species. Thus, the relatively low oxygen demands of this low-activity species are likely amply met by their available gill area and metabolic rate is able to scale isometrically with body mass (Fig. 2-1a). Additionally, according to the gill oxygen limitation theory, if gill area were limiting metabolic rate, we would not see isometric scaling of RMR and hyperallometric scaling of MMR as we do here (Figs 2-1b, 2-4) (Pauly, 2021; Pauly and Cheung, 2017). While MMR slope values near or above isometry have been found in other fish species, the significantly hyperallometric (>1) slope found here in California Horn Shark is unusual (Brett and Glass, 1973; Goolish, 1991). The increase in aerobic scope as body mass increases suggests that the lifestyle of a larger individual requires a significantly greater capacity

for activity above rest – juvenile California Horn Shark appear to prefer relatively shallow and sandy habitats where they likely feed on soft-bodied invertebrate prey, while adult individuals occupy rocky reefs and are known to travel up to 13km in a single night of hunting (Compagno, 2002; Cortés-Fuentes et al., 2020; Meese and Lowe, 2020). These findings suggest we may need to consider activity level when modeling metabolic rate and energy-based ecological processes.

We can see how isometric scaling of gill area may be achieved by examining the scaling of the gill components, specifically filament length, lamellar frequency, and lamellar surface area (Fig. 2-5). If gill area is to increase geometrically with body mass as the fish grows, the expected slope is surface area/volume which is 2/3 or 0.67, yet the observed slope is 0.888 ± 0.077 across the full sample size range and 1.014 ± 0.151 across adults (Fig. 1a) (Wegner, 2016). Again from a geometric expectation, the scaling of filament length, lamellar frequency, and lamellar surface area are predicted to be 0.33 (length/volume), -0.33 (length^{-1}/volume), and 0.67 (surface area/volume), respectively, to sum to a total of 0.67 (Wegner, 2016). Here, the California Horn Shark achieves gill area isometry by increasing filament length and lamellar surface area and by maintaining lamellar density. Specifically, filament length increases with body mass with a slope significantly steeper than 0.33 (slope = 0.404 ± 0.019) and lamellar frequency decreases with a slope significantly shallower than -0.33 (slope = -0.101 ± 0.013). Similar to gill area, lamellar surface area may scale with an inflection point near the point of maturation (the third smallest individual, Fig. 2-5). When modeled with a broken stick regression, the allometric slope of lamellar surface area at the larger body masses is 0.741 ± 0.091, which is not significantly greater than 0.67. However, when combined with the slopes of filament length and lamellar frequency, it provides a pathway for the slope of gill area to scale near-isometrically (0.404 - 0.101 + 0.741 = 1.044). This pattern of gill component scaling is consistent with those of other elasmobranchs, where we see adjustments in the slope values of each gill component to reach a sum total of the species' particular gill area scaling exponent (Wegner, 2016). For example, gill area in the Common Thresher Shark (*Alopias vulpinus*) has been shown to scale with an exponent of 1.03 across a body size range of 7.9–91.5 kg (Wootton et al., 2015). This is achieved through a significant increase in lamellar area (slope = 0.86) and a relatively small reduction in lamellar frequency (slope = -0.16) throughout ontogeny (Wootton et al., 2015). Additionally, for California Horn Shark, an inflection point at the same location

for both gill area and lamellar surface area hints that the slope of gill area and body mass may be largely influenced by changes in lamellar surface area, where the growth of the lamellae themselves may slow upon hatching to shift the gill area to align with metabolic demand. Lamellar area has been shown to be the more plastic gill component in the face of hypoxia, supporting the hypothesis that this is the component which augments to accommodate rapid changes in gill area in California Horn Shark (Sollid and Nilsson, 2006; Wegner, 2016).

Our findings are a first look at the allometric scaling patterns of gill surface area, maximum and resting metabolic rates using paired estimates within the same individuals. Taken together, our results suggest that when a species' oxygen demand is relatively low, like in a small inactive species – the California Horn Shark – the allometric scaling of gill area can overcome surface area-to-volume constraints and the allometric scaling of metabolic rate can be isometric or above. Additionally, the inflection point found in the scaling of gill area as a function of body mass highlights the importance of using a complete body-size range when generating an allometric slope. Our findings regarding a potential inflection point in the ratio of gill area to metabolic rate across body mass further confirm the importance of a complete size range. This is an exciting avenue within which to test the possibilities of oxygen limitation, as extremely few studies have truly explored the relationship between gills and metabolic rate across a complete size range. Finally, the unusually steep scaling exponents found here emphasize the need for more work examining these traits in species of varying activity levels and ecological lifestyles.

2.6. References

Bigman, J. S., Pardo, S. A., Prinzing, T. S., Dando, M., Wegner, N. C. and Dulvy, N. K. (2018). Ecological lifestyles and the scaling of shark gill surface area. *J. Morphol.* 279, 1716–1724.

Bishop, C. M. (1999). The maximum oxygen consumption and aerobic scope of birds and mammals: Getting to the heart of the matter. *Proc. R. Soc. B Biol. Sci.* 266, 2275–2281.

Bokma, A. F. (2004). Evidence against Universal Metabolic Allometry. *Funct. Ecol.* 18, 184–187.

Brett, J. R. and Glass, N. R. (1973). Metabolic Rates and Critical Swimming Speeds of Sockeye Salmon (*Oncorhynchus nerka*) in Relation to Size and Temperature. *J. Fish. Res. Board Canada* 30, 379–387.

Brown, J. H., Gillooly, J. F., Allen, A. P., Savage, V. M. and West, G. B. (2004). Toward a metabolic theory of ecology. *Ecology* 85, 1771–1789.

Chabot, D., Steffensen, J. F. and Farrell, A. P. (2016). The determination of standard metabolic rate in fishes. *J. Fish Biol.* 88, 81–121.

Cheung, W. W. L., Sarmiento, J. L., Dunne, J., Frölicher, T. L., Lam, V. W. Y., Palomares, M. L. D., Watson, R. and Pauly, D. (2013). Shrinking of fishes exacerbates impacts of global ocean changes on marine ecosystems. *Nat. Clim. Chang.* 3, 254–258.

Clark, T. D., Sandblom, E. and Jutfelt, F. (2013). Aerobic scope measurements of fishes in an era of climate change: respirometry, relevance and recommendations. *J. Exp. Biol.* 216, 2771–2782.

Compagno, L. J. V. (2002). Order Heterodontiformes - Bullhead sharks. In *Sharks of the World, Vol. 2*, pp. 31–50. Food and Agriculture Organization of the United Nations.

Cortés-Fuentes, C., Simental-Anguiano, M. del R., Galván-Magaña, F. and Medina-López, M. A. (2020). Feeding habits of the horn shark Heterodontus francisci (Girard, 1855) in the northwest of Baja California Sur, Mexico. *J. Appl. Ichthyol.* 36, 197–202.

De Jager, S. and Dekkers, W. (1975). Relations between gill structure and activity in fish. *Netherlands J. Zool.* 25, 276–308.

Deutch, C., Ferrel, A., Seibel, B., Pörtner, H. O. and Huey, R. B. (2015). Climate change tightens a metabolic constraint on marine habitats. *Science.* 348, 1132–1136.

Di Santo, V., Tran, A. H. and Svendsen, J. C. (2016). Progressive hypoxia decouples activity and aerobic performance of skate embryos. *Conserv. Physiol.* 4, 1–7.

Ebert, D. A., Fowler, S., Compagno, L. and Dando, M. (2013). *Sharks of the World*. Wild Nature Press.

Ern, R., Huong, D. T. T., Cong, N. V., Bayley, M. and Wang, T. (2014). Effect of salinity on oxygen consumption in fishes: A review. *J. Fish Biol.* 84, 1210–1220.

Evans, D. H., Piermarini, P. M. and Choe, K. P. (2005). The multifunctional fish gill: Dominant site of gas exchange, osmoregulation, acid-base regulation, and excretion of nitrogenous waste. *Physiol. Rev.* 85, 97–177.

Gillooly, J. F., Brown, J. H., West, G. B., Savage, V. M. and Charnov, E. L. (2001). Effects of Size and Temperature on Metabolic Rate. *Science.* 293, 2248–2251.

Gillooly, J. F., Gomez, J. P., Mavrodiev, E. V., Rong, Y. and McLamore, E. S. (2016). Body mass scaling of passive oxygen diffusion in endotherms and ectotherms. *Proc. Natl. Acad. Sci.* 113, 5340–5345.

Glazier, D. S. (2005). Beyond the “3/4-power law”: Variation in the intra- and interspecific scaling of metabolic rate in animals. *Biol. Rev. Camb. Philos. Soc.* 80, 611–662.

Glazier, D. S. (2009). Activity affects intraspecific body-size scaling of metabolic rate in ectothermic animals. *J. Comp. Physiol. B Biochem. Syst. Environ. Physiol.* 179, 821–828.

Glazier, D. S. (2010). A unifying explanation for diverse metabolic scaling in animals and plants. *Biol. Rev.* 85, 111–138.

Goolish, E. M. (1991). Aerobic and anaerobic scaling in fish. *Biol. Rev. Camb. Philos. Soc.* 66, 33–56.

Graham, J. B. and Laurs, R. M. (1982). Metabolic Rate of the Albacore Tuna Thunnus alalunga. *Mar. Biol.* 72, 1–6.

Hughes, G. M. (1972). Morphometrics of Fish Gills. In *Respiration Physiology*, pp. 1–25.

Hughes, G. M. (1984). Scaling of respiratory areas in relation to oxygen consumption of vertebrates. *Experientia* 40, 519–524.

Jerde, C. L., Kraskura, K., Eliason, E. J., Csik, S. R., Stier, A. C. and Taper, M. L. (2019). Strong Evidence for an Intraspecific Metabolic Scaling Coefficient Near 0.89 in Fish. *Front. Physiol.* 10, 1–17.

Killen, S. S., Costa, I., Brown, J. A. and Gamperl, A. K. (2007). Little left in the tank: Metabolic scaling in marine teleosts and its implications for aerobic scope. *Proc. R. Soc. B Biol. Sci.* 274, 431–438.

Killen, S. S., Atkinson, D. and Glazier, D. S. (2010). The intraspecific scaling of metabolic rate with body mass in fishes depends on lifestyle and temperature. *Ecol. Lett.* 13, 184–193.

Killen, S. S., Glazier, D. S., Rezende, E. L., Clark, T. D., Atkinson, D., Willener, A. S. T. and Halsey, L. G. (2016). Ecological Influences and Morphological Correlates of Resting and Maximal Metabolic Rates across Teleost Fish Species. *Am. Nat.* 187, 592–606.

Kleiber, M. (1932). Body size and metabolism. *Hilgardia* 6, 315–332.

Lefevre, S., McKenzie, D. J. and Nilsson, G. E. (2017). Models projecting the fate of fish populations under climate change need to be based on valid physiological mechanisms. *Glob. Chang. Biol.* 23, 3449–3459.

Lenth, R., Buerkner, P., Herve, M., Love, J., Riebl, H. and Singmann, H. (2020). emmeans: Estimated Marginal Means, aka Least-Squares Means. R package version 1.4.8. https://CRAN.R-project.org/package=emmeans.

Li, G., Lv, X., Zhou, J., Shen, C., Xia, D., Xie, H. and Luo, Y. (2018). Are the surface areas of the gills and body involved with changing metabolic scaling with temperature? *J. Exp. Biol.* 221, jeb174474.

Luo, Y., He, D., Li, G., Xie, H., Zhang, Y. and Huang, Q. (2015). Intraspecific metabolic scaling exponent depends on red blood cell size in fishes. *J. Exp. Biol.* 218, 1496–1503.

Luo, Y., Li, Q., Zhu, X., Zhou, J., Shen, C., Xia, D., Djiba, P. K., Xie, H., Lv, X., Jia, J., et al. (2020). Ventilation frequency reveals the roles of exchange surface areas in metabolic scaling. *Physiol. Biochem. Zool.* 93, 13–22.

Luongo, S. M. and Lowe, C. G. (2018). Seasonally acclimated metabolic Q10of the California horn shark, *Heterodontus francisci*. *J. Exp. Mar. Bio. Ecol.* 503, 129–135.

Meese, E. N. and Lowe, C. G. (2020). Active acoustic telemetry tracking and tri- axial accelerometers reveal fine-scale movement strategies of a non-obligate ram ventilator. *Mov. Ecol.* 8, 1–17.

Muggeo, V. M. R. (2003). Estimating regression models with unknown break-points. *Stat. Med.* 22, 3055–3071.

Muggeo, V. M. R. (2008). Modeling temperature effects on mortality: Multiple segmented relationships with common break points. *Biostatistics* 9, 613–620.

Muir, B. S. and Hughes, G. M. (1969). Gill dimensions for three species of tunny. *J. Exp. Biol.* 51, 271–285.

Nilsson, G. E. and Östlund-Nilsson, S. (2008). Does size matter for hypoxia tolerance in fish? *Biol. Rev.* 83, 173–189.

Norin, T. and Gamperl, A. K. (2017). Metabolic scaling of individuals vs. populations: Evidence for variation in scaling exponents at different hierarchical levels. *Funct. Ecol.* 32, 379–388.

Pauly, D. (1981). The relationships between gill surface area and growth performance in fish: a generalization of von Bertalanffy's theory of growth. *Reports Mar. Res.* 28, 251–282.

Pauly, D. (2010). Gasping fish and panting squids: Oxygen, temperature and the growth of water-breathing animals. *Excell. Ecol.* 22, 1–247.

Pauly, D. (2021). The gill-oxygen limitation theory (GOLT) and its critics. *Sci. Adv.* 7, 1–19.

Pauly, D. and Cheung, W. W. L. (2017). Sound physiological knowledge and principles in modeling shrinking of fishes under climate change. *Glob. Chang. Biol.* 24, e15–e26.

Pörtner, H. O. and Knust, R. (2007). Climate change affects marine fishes through the oxygen limitation of thermal tolerance. *Science.* 315, 95–97.

Post, J. R. and Lee, J. A. (1996). Metabolic ontogeny of teleost fishes. *Can. J. Fish. Aquat. Sci.* 53, 910–923.

Powter, D. M., Gladstone, W. and Platell, M. (2010). The influence of sex and maturity on the diet, mouth morphology and dentition of the Port Jackson shark, Heterodontus portusjacksoni. *Mar. Freshw. Res.* 61, 74–85.

Reidy, S. P., Nelson, J. A., Tang, Y. and Kerr, S. R. (1995). Post-exercise metabolic rate in Atlantic cod and its dependence on the method of exhaustion. *J. Fish Biol.* 47, 377–386.

Rodda, K. R. and Seymour, R. S. (2008). Functional morphology of embryonic development in the Port Jackson shark Heterodontus portusjacksoni (Meyer). *J. Fish Biol.* 72, 961–984.

Rodgers, G. G., Tenzing, P. and Clark, T. D. (2016). Experimental methods in aquatic respirometry: The importance of mixing devices and accounting for background respiration. *J. Fish Biol.* 88, 65–80.

Rombough, P. J. and Moroz, B. M. (1997). The scaling and potential importance of cutaneous and branchial surfaces in respiratory gas exchange in larval and juvenile walleye Stizostedion vitreum. *J. Exp. Biol.* 200, 2459–2468.

Rubalcaba, J. G., Verberk, W. C. E. P., Hendriks, A. J., Saris, B. and Woods, H. A. (2020). Oxygen limitation may affect the temperature and size dependence of metabolism in aquatic ectotherms. *Proc. Natl. Acad. Sci.* In press, 1–6.

Savage, V. M., Gillooly, J. F., Woodruff, W. H., West, G. B., Allen, A. P., Enquist, B. J. and Brown, J. H. (2004). The predominance of quarter-power scaling in biology. *Funct. Ecol.* 18, 257–282.

Sollid, J. and Nilsson, G. E. (2006). Plasticity of respiratory structures - Adaptive remodeling of fish gills induced by ambient oxygen and temperature. *Respir. Physiol. Neurobiol.* 154, 241–251.

Svendsen, M. B. S., Bushnell, P. G. and Steffensen, J. F. (2016). Design and setup of intermittent-flow respirometry system for aquatic organisms. *J. Fish Biol.* 88, 26–50.

Toulmond, A. (1982). Cutaneous O2 and CO2 exchanges in the dogfish, Scyliorhinus canicula. *Respir. Physiol.* 48, 169–181.

Wegner, N. C. (2011). *Ventilation and animal respiration* | *Gill Respiratory Morphometrics*. Elsevier Inc.

Wegner, N. C. (2016). Elasmobranch Gill Structure. In *Physiology of Elasmobranch Fishes: Structure and Interaction with Environment.* (ed. Shadwick, R. E., Farrell, A. P., and Brauner, C. J.), pp. 101–151. New York City, NY: Academic Press.

Wegner, N. C., Sepulveda, C. A., Olson, K. R., Hyndman, K. A. and Graham, J. B. (2010). Functional morphology of the gills of the shortfin mako, Isurus oxyrinchus, a lamnid shark. *J. Morphol.* 271, 937–948.

Wootton, T. P., Sepulveda, C. A. and Wegner, N. C. (2015). Gill morphometrics of the thresher sharks (Genus *Alopias*): Correlation of gill dimensions with aerobic demand and environmental oxygen. *J. Morphol.* 276, 589–600.

Zhang, Y., Huang, Q., Liu, S., He, D., Wei, G. and Luo, Y. (2014). Intraspecific mass scaling of metabolic rates in grass carp (*Ctenopharyngodon idellus*). *J. Comp. Physiol. B Biochem. Syst. Environ. Physiol.* 184, 347–354.

Chapter 3.

Statistical methods matter too: Establishing a framework for estimating maximum metabolic rate for fishes[2]

3.1. Abstract

Advances in experimental design and equipment have simplified the collection of maximum metabolic rate (MMR) data for a more diverse array of water-breathing animals. However, little attention has been paid to the consequences of statistical choices on the estimation of MMR. This may reduce the comparability of estimates across species and studies and has consequences for the burgeoning number of metanalyses using metabolic rate data. Two key statistical choices that require standardization are the time interval, or regression window width, over which MMR is estimated and the method used to locate that regression window within the raw oxygen depletion trace. Here, we consider the effect of both choices by estimating MMR for two shark and two salmonid species of different activity levels using multiple regression window widths and three statistical methods: rolling regression, sequential regression, and segmented regression. We then compared these estimates within each species. Shorter regression windows yielded higher metabolic rate estimates, with a risk that the shortest windows (< 1-minute) reflect more system noise than MMR signal. Rolling regression was the best candidate model and produced the highest MMR estimates. Sequential regression models consistently produced lower relative estimates than the compared rolling regression models, while the segmented regression model was unable to produce consistent MMR estimates across individuals. The time-point of the MMR regression window along the oxygen consumption trace varied considerably across individuals but not across models. We show that statistical choices, in addition to more widely understood experimental choices, profoundly affect the resultant estimates of

[2] A version of this chapter is accepted for publication as:

Prinzing, T.S., Zhang, Y., Wegner, N.C., Dulvy, N.K. (2021) Analytical methods matter too: Establishing a framework for estimating maximum metabolic rate for fishes. *Ecology and Evolution.*

MMR. We recommend that researchers (1) employ a rolling regression model with a 1- to 2-minute regression window, depending on experimental system and (2) explicitly report their analytical methods, publishing raw data and code, and that journal editors are aware that these MMR measurements depend on arbitrary choices requiring sensitivity testing.

3.2. Introduction

Metabolic rate is the rate at which organisms convert food and materials from their environment into energy to fuel their biological processes. Metabolic rate is thus the fundamental rate of life, and is a key indicator of physiological performance across tissues, cells and whole organisms (Brown et al., 2004; White and Kearney, 2013). Examination of metabolic rate is becoming increasingly popular within the fields of ecology and comparative physiology as a tool to link organismal physiology to population, community and ecosystem phenomena, and to help us understand and make predictions about vulnerable species, diverse ecosystems, and climate change (Barneche et al., 2014; Deutch, Ferrel, Seibel, Pörtner, & Huey, 2015; Pörtner, Bock, & Mark, 2017). Standard or resting metabolic rate is often used in meta-analyses as it is simpler to estimate than routine or maximum metabolic rate. However, recent work has drawn additional attention to the ecological importance of estimating metabolic rate during these higher levels of energy expenditure as they may better characterize organismal daily energy budgets and physiological constraints (Deutch et al., 2015; Glazier, 2005; Killen et al., 2016).

Maximum metabolic rate (MMR) is usually defined as the highest metabolic rate attainable by an organism and is typically associated with exhaustive exercise (Norin & Clark, 2016). In fishes, MMR is typically measured and expressed through the proxy measurement of oxygen consumption following exercise or air exposure, and the standardization of experimental methods is improving as a growing number of studies outline the design and set-up of associated respirometry experiments (Cech Jr. & Brauner, 2011; Clark, Sandblom, & Jutfelt, 2013; Payne et al., 2015; Svendsen, Bushnell, & Steffensen, 2016). However, the quantitative process of actually estimating MMR from the experimental oxygen consumption data has yet to be tested or

standardized, despite recognition that statistical choices affect MMR estimates (Norin & Clark, 2016; Zhang, Gilbert, & Farrell, 2019, 2020). Often, details on the statistical approach used to estimate MMR are not clearly reported, and when provided, there is usually little or no explanation as to why those specific methods were chosen. These unknowns and lack of consistency potentially bias MMR estimates and makes comparison between studies difficult.

Respirometry experiments used to estimate MMR measure the rate of oxygen depletion from a closed pool of water containing the test individual, and then fit a regression to the change in oxygen concentration as a function of time (Svendsen et al. 2016). For estimating MMR, a change in the amount of time over which maximum oxygen consumption is measured (specifically, the width of the regression window) may change the slope of this relationship and the resulting MMR estimate (Norin & Clark, 2016). This is because MMR is an unsustainably high level of energy expenditure, usually occurring in response to burst exercise, and thus likely occurs over a relatively short window of time. Too long a window width can incorporate periods of lower energy expenditure, depressing the MMR estimate. Conversely, noise, brief spikes and inherent error in experimental systems set a minimum limit on window width (Zhang, et al., 2019). Despite this trade-off, there is currently no widely accepted method for selecting a suitable window width. The window widths used in analyses vary across studies, and may even go unreported; 1 to 5 minutes is common, but much longer windows are not unusual (e.g. 10 and 15 minutes) (Killen et al., 2007; Závorka et al., 2018). In some cases, the window width is tailored to each individual and thus varies across individuals within a study. However, the degree to which MMR estimates are affected by the choice of regression window width, and under what experimental conditions, is unknown. More work is needed to determine if this choice effects MMR to the point of significantly changing estimates, study conclusions, and comparability of estimates across studies.

There are two common statistical methods for analyzing MMR data in aquatic respirometry: rolling regression and sequential regression. Rolling regression is growing in popularity because the overlapping regression windows and extremely high resolution reduce the chance of missing the MMR window, and this method is simple to implement with common programming software such as Excel, R, and Labchart (Fig. 3-1a) (Harianto et al., 2019; Zhang et al., 2019). By comparison, sequential regression is a more traditional method and works by placing regression windows of a set width end-to-

end along the full set of raw oxygen depletion data, limiting the placement of each regression window to a much smaller subset within the oxygen depletion trace (Fig. 3-1b) (Tirsgaard et al., 2015; Zhang et al., 2019). In addition to these commonly used methods, a third model, segmented regression (sometimes termed broken-stick regression), may be useful in taking advantage of the generally unstable nature of oxygen depletion traces immediately post exercise (Fig. 3-1f). This model is typically used to estimate hypoxia tolerance or critical oxygen tension in aquatic ectotherms, but has not previously been used to estimate MMR (Reemeyer and Rees, 2019; Slesinger et al., 2019). For this model, we hypothesized that the beginning and end of each MMR window would be marked by a change in the rate of oxygen consumption, detectable as "break-points" that define the unique location and width of the MMR window for each individual. However, like window width itself, the suitability and effect of each of these models for the estimation of MMR has yet to be thoroughly tested.

Here, we first estimated MMR and its time-point within the oxygen depletion trace for two shark and two salmonid species using each of these statistical methods: rolling regression, sequential regression, segmented regression. This allowed us to test the effectiveness of each statistical approach across a variety of life histories: an inactive benthic shark, a demersal shark of medium activity level, and two relatively high activity level pelagic salmonids. We estimated MMR using multiple window widths within both rolling and sequential regression models to test for the effect of window width on MMR estimate. Second, we compared the resulting MMR estimates from all models within and across each species. Third, because the relationship between metabolic rate and body mass is foundational to the theories behind aerobic scope and metabolic ecology (Brown et al., 2004; Clark et al., 2013), we also tested the effect of model choice on the allometry of MMR and body mass for the California Horn Shark (*Heterodontus francisci*, our inactive benthic shark species), for which data were collected over a wide body size range. We sought a model that (1) was easily applied to data from a variety of species, (2) relied on the least amount of subjective decision making, and (3) produced MMR estimates with reasonably low variance across individuals. This work demonstrates the importance of considering statistical methods when estimating MMR and provides a framework with which to approach analysis.

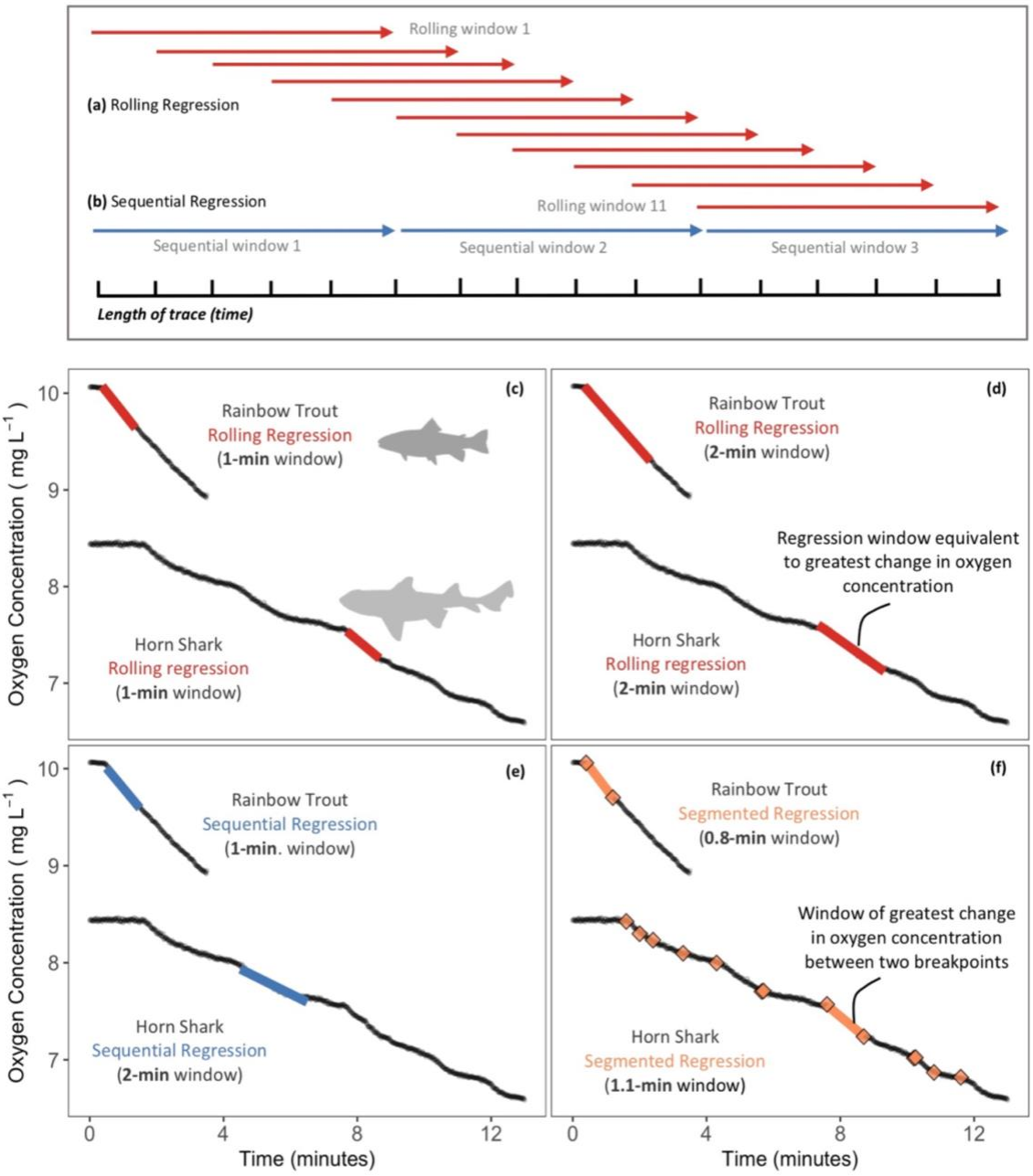
Rolling window 1
(a) Rolling Regression
(b) Sequential Regression
Rolling window 11
Sequential window 1
Sequential window 2
Sequential window 3
Length of trace (time)
(c)
Rainbow Trout
Rolling Regression
(1-min window)
Horn Shark
Rolling regression
(1-min window)
(d)
Rainbow Trout
Rolling Regression
(2-min window)
Regression window equivalent to greatest change in oxygen concentration
Horn Shark
Rolling regression
(2-min window)
(e)
Rainbow Trout
Sequential Regression
(1-min. window)
Horn Shark
Sequential Regression
(2-min window)
(f)
Rainbow Trout
Segmented Regression
(0.8-min window)
Window of greatest change in oxygen concentration between two breakpoints
Horn Shark
Segmented Regression
(1.1-min window)
Oxygen Concentration (mg L^{-1})
10
9
8
7
0
4
8
12
Time (minutes)

Figure 3-1 **Conceptual schematic of the sampling window for rolling (a) and sequential (b) regression windows and the application of rolling (c-d), sequential (e), and segmented (e) regressions to raw oxygen data used to estimate maximum metabolic rate. (a) Rolling regression windows overlap by one timestep estimating all possible Ordinary Least Squares regressions across the oxygen consumption trace. (b) Sequential regression windows have no overlap and line up end-to-end across the oxygen consumption trace. (c-f) Raw oxygen consumption traces of example individual Rainbow Trout (0.088 kg body mass, 2.25 L chamber vol.) and California Horn Shark (1.7 kg body mass, 30.2 L chamber vol.) over time showing where the respective model estimates the regression window to occur. (c-d) Rolling regression with a 1-and 2-min regression window, respectively, (e) sequential regression with a 1-min window for Rainbow Trout and a 2-min window for California Horn Shark, and (f) segmented regression with estimated breakpoint locations indicated by colored points. (a) and (b) are inspired by Fig. 2 in Harianto, Carey and Byrne (2019).**

3.3. Methods

We collated maximum metabolic rate (MMR) data sets from a sedentary benthic elasmobranch, the California Horn Shark, *Heterodontus francisci* (Girard 1855) (n = 17, 0.203–4.46 kg), a demersal shark of medium activity, the Gray Smoothhound *Mustelus californicus* (Gill 1864) (n = 4, 0.76–1.6 kg), and two highly active salmonid species, the Rainbow Trout *Oncorhynchus mykiss* (Walbaum 1792) (n = 16, 0.06–0.11 kg, Zhang, Gilbert, & Farrell, 2020), and Atlantic Salmon *Salmo salar* (Linnaeus 1758) (n = 20, 0.06–0.12 kg, Zhang et al., 2016). Data for sharks were collected using relatively large individuals across a wide body size range, while data for salmonids were collected using relatively small juveniles. All data were collected using intermittent flow respirometry and a chase-to-exhaustion protocol (see Appendix for further detail). Each protocol resulted in a single oxygen depletion trace for each individual (e.g. Fig. 3-1 c-f). We then used each of three statistical methods to estimate MMR for each individual: (1) rolling regression with 1-to 5-minute sampling window widths, (2) sequential regression with 1- and 2-minute window widths, and (3) segmented regression. MMR was estimated by fitting a regression model (see specifics for each model below) to different windows of time across the oxygen consumption trace and searching for the highest slope. The slope of this regression (β_{O_2}) was then used to calculate oxygen consumption (M_{O_2}) using the equation

$$M_{O_2} = [(V_r - V_f) \times \beta_{O_2}] \ / \ M_f \qquad (1)$$

where V_r is the respirometer chamber volume in litres, V_f is the fish volume (assumed to be equivalent to the fish mass, M_f). Additionally, we estimated the time-point at which MMR occurred along each individual oxygen consumption trace. All statistical analyses were carried out in R (R version 3.6.3 (2020-02-29)).

We tested the effectiveness of a signal-to-noise ratio analysis method in determining an appropriate regression window width to use in the analysis of MMR data (Zhang et al., 2019, 2020). Details and results of this analysis are included in Appendix B.

3.3.1. Rolling regression

A rolling regression model runs all possible Ordinary Least Squares regressions of a specified window width across a data set, stepping forward by one data point at a time (Fig. 3-1a) (Harianto & Carey, 2019). This greatly reduces the chance of missing the MMR window assuming it was recorded in the data set. For example, a ten-min oxygen depletion trace, where oxygen concentration was measured every second, would result in 541 1-min or 481 2-min regression estimates.

We applied a rolling regression model across the full measurement cycle for each individual by applying the function `roll_regress()` from the *rollRegres* package (Christoffersen, 2019, version 0.1.3). This model results in a dataset of regression coefficients, one row for each individual regression. From this, we selected the single regression window producing the steepest slope coefficient and used this to estimate MMR with Equation 1. We used this model to estimate MMR for each of 1-, 2-, and 3-min regression window widths for salmonids (their oxygen consumption was measured over a shorter, 3.5-4.5 min time period), and 1-, 2-, 3-, and 5-min regression window width for sharks (their oxygen consumption was measured over a longer 10-12 min time period), thus producing three estimates of MMR for salmonids and four for sharks. These window widths were chosen as they are commonly used to study MMR in fishes and allowed us to compare the effects of window width on MMR estimation (Auer, Salin, Anderson, & Metcalfe, 2018; Norin & Clark, 2016; Roche, Binning, Bosiger, Johansen, & Rummer, 2013).

3.3.2. Sequential regression

MMR was also estimated for each fish using a sequential regression model where regression lines were placed end-to-end along each oxygen consumption trace (Fig. 3-1b). For each individual, a 30-s “lag period” was removed from the beginning of each trace. This lag arises because of the time delay until oxygen-depleted water expelled from the fish’s gills circulates past and is recorded by the oxygen meter probe. The use of a lag period was not necessary for the segmented and rolling regression models because these model’s high resolution naturally accounts and adjusts for this lag period. The first regression window was then placed at this corrected start time, using a 1-min regression window for salmonids and both a 1- and 2-min window for sharks. We

were limited by the time over which oxygen consumption was measured for salmonids (3.5-4.5 min) and were only able to use a 1-min regression window for them in this analysis. Slopes of oxygen consumption over time were estimated for each sequential time window, moving across the MMR trace by one regression window width with no overlapping data used (Fig. 3-1b, e). The regression window yielding the steepest slope was then used to estimate MMR.

3.3.3. Segmented regression

Segmented regression estimates breakpoints that are changes in the relationship between the predictor and response variables, as well as the distance between these points. Applied to respirometry data, a segmented model can estimate breakpoints that represent changes in the rate of oxygen consumption over time, and the distance between each breakpoint gives us a regression window. We ran an iterative segmented regression model on each oxygen depletion trace for each individual to estimate a unique regression window using the `segmented()` function from the package *segmented* (Muggeo, 2003, 2008, version 1.2.0). The slope of the regression of oxygen consumption as a function of time over this regression window was then used to estimate MMR.

To estimate a regression window for each individual, we repeatedly applied the segmented regression model to each oxygen depletion trace to estimate an iteratively increasing number of breakpoints. The model starts by estimating a single breakpoint in the rate of oxygen consumption over time, then two break points, three, and so on until no more breakpoints can be estimated. Each iteration of the model is a completely independent estimate of the number and locations of breakpoints, meaning they can occur at different locations than in earlier iterations of the model. We used the iteration of the model yielding the sampling window with the steepest slope coefficient to estimate MMR for that individual, irrespective of the total number of breakpoints estimated. Because the segmented regression model estimates breakpoints where it detects a significant change in the rate of oxygen consumption, sometimes placing breakpoints extremely close to one another, it was necessary to specify a minimum acceptable window width to prevent unreasonably high MMR estimates, caused by spurious changes in oxygen concentration or measurement error, from occurring. The 90% detection confidence limit of our oxygen meters was 40 s, and this was the only variance

within our experimental system we could quantify confidently. Hence, we set 45s between breakpoints as a more conservative minimum regression window and we removed slope coefficients from our output data frame that corresponded to window widths shorter than this.

3.3.4. Comparison among models

We tested for the effect of model on MMR estimate within each species. Each MMR estimate was standardized to mean body mass for California Horn Shark (1.95 kg), Rainbow Trout (0.073 kg), and Atlantic Salmon (0.092 kg). To do this, we calculated residual MMR values as the difference between the measured and predicted MMR value within each species according to the relationship between MMR and body mass ($MMR = a M^{b}$, where a and b are constants calculated for each model for each species, and M is body mass) (Norin, Malte, & Clark, 2016; Xiao, White, Hooten, & Durham, 2011). Residual values were normally distributed (Shapiro-Wilk, $p > 0.05$) for all models. For each individual, we then added the raw residual MMR value (positive or negative) to the predicted MMR value at the mean body mass for each species to standardize the absolute MMR to the species-specific mean body mass. Due to the small number of individuals tested in this study (n=4), Gray Smoothhound were not quantitatively analyzed as we were not able to standardize their estimates and we instead reported their estimates unstandardized as mass-specific values.

To test for the effect of model on MMR estimate within each species (California Horn Shark and salmonids), we fit a linear mixed effects model with standardized MMR estimate as a function of model name with individual identity as a random effect (Bates, Maechler, Bolker & Walker, 2015). We then compared between mean values for each model and account for multiple comparisons and unequal variance using the `emmeans()` function (Lenth, 2020).

Along with each MMR estimate, we estimated the timepoint along the oxygen consumption trace when the MMR window was identified for each individual for each model, measured as time from first placement in the respirometer chamber to the midpoint of each regression window. We tested for the effect of model on window location by fitting a linear mixed effects model with window location as a function of model name with individual identity as a random effect (Bates et al., 2015). We then

compared between mean window location values for each model and account for multiple comparisons and unequal variance using the `emmeans()`function (Lenth, 2020).

Because California Horn Shark data were collected using animals across a wide body-size range, we were able to test for the effect of model on the slope estimate of log MMR as a function of log body mass. We fit a linear mixed effects model with log MMR as a function of log body mass, with model as an interaction term and individual as a random effect, then compared across slope estimates and accounted for multiple comparisons using the `emtrends()` function (Lenth, 2020).

3.4. Results

3.4.1. How does the choice of window width and regression model affect the MMR estimate?

Shorter regression window widths yielded higher MMR estimates in all species (Fig. 3-2, B-1, Table 3-1). In pair-wise comparisons between adjacent models, the largest difference occurred between the shortest window widths, where the 1-min window rolling regression model mean MMR estimates were 36%, 7% and 5% higher than the 2-min window rolling regression model mean MMR estimates for California Horn Shark, Rainbow Trout and Atlantic Salmon respectively (Fig. 3-2). As window width increased, both the relative difference in mean MMR estimate between subsequent models and the standard deviation around the mean MMR estimate decreased.

Across all models, the 1-minute window rolling regression model produced the highest MMR estimates in all species, followed by estimates made with the segmented regression model (Fig 3-2, Fig. B-1, Table 3-1). Mean MMR estimates for the segmented regression model were higher than California Horn Shark 2-min window and Atlantic Salmon 1-minute window sequential regression models, however, there was also considerably higher variance around the California Horn Shark segmented regression mean MMR estimate (Fig. 3-2, Table 3-1). In all species, the sequential regression models produced lower mean MMR estimates compared to their corresponding window width rolling regression models, where California Horn Shark 1-and 2-min, Rainbow Trout 1-min and Atlantic Salmon 1-min sequential regression model estimates were 22%, 24%, 3% and 4% lower, respectively (Fig. 3-2, Table 3-1).

Differences across window widths and models were considerably larger for California Horn Shark than for salmonids (Table 3-1, Fig 3-2, Fig. B-1). California Horn Shark mean body mass was 23 times larger than the mean body mass of the salmonids (1.95 kg and 0.083 kg, respectively), and considerably larger chamber sizes were used to measure oxygen consumption. California Horn Shark oxygen consumption traces at larger body masses and chamber sizes were often more variable compared to traces at smaller body masses and to salmonid traces (Fig. 3-1c-f).

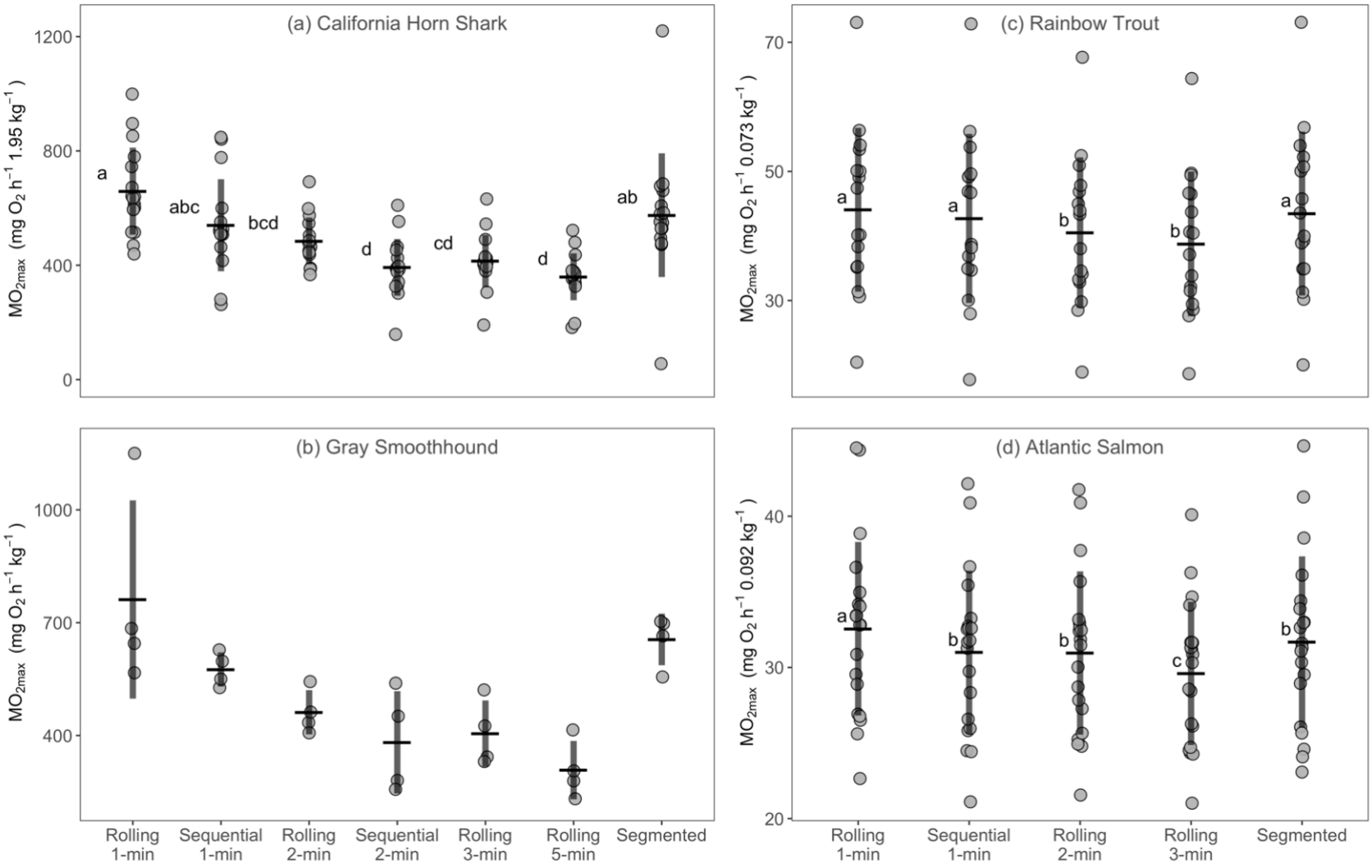
(a) California Horn Shark
(b) Gray Smoothhound
(c) Rainbow Trout
(d) Atlantic Salmon
MO2max (mg O2 h-1 1.95 kg-1)
MO2max (mg O2 h-1 kg-1)
MO2max (mg O2 h-1 0.073 kg-1)
MO2max (mg O2 h-1 0.092 kg-1)
Rolling 1-min
Sequential 1-min
Rolling 2-min
Sequential 2-min
Rolling 3-min
Rolling 5-min
Segmented

Figure 3-2 **Mean MMR estimate decreased with increasing regression window width. Rolling and sequential regression window width used is indicated by the time listed (e.g., 1-min) in each model label. Sequential regression model mean MMR estimates were lower than those estimated with equivalent window width rolling regression models in all cases. Unique letters indicate significance level of $P < 0.05$ between compared models. Each species' MMR estimates were standardized to the mean species mass before analysis (see y-axis), except Gray Smoothhound which are reported as mass-specific values. Means are reported ± SD.**

	California Horn Shark		Rainbow Trout		Atlantic Salmon		Scaling of MMR and body mass for California Horn Shark	
Model Comparison	**Estimate**	**p-value**	**Estimate**	**p-value**	**Estimate**	**p-value**	**Estimate**	**p-value**
Rolling 1-min - Rolling 2-min	174.3630	0.0010	3.5566	0.0001	1.6097	0.0000	0.1234	0.2043
Rolling 1-min - Rolling 3-min	244.7367	0.0000	5.2880	0.0000	2.9648	0.0000	0.1835	0.0093
Rolling 1-min - Rolling 5-min	299.6471	0.0000	—	—	—	—	0.2162	0.0011
Rolling 1-min - Segmented	64.9517	0.3973	0.5185	0.9318	0.7357	0.0197	0.0523	0.9917
Rolling 1-min - Sequential 1-min	119.1873	0.0681	1.3403	0.3681	1.5667	0.0000	0.0647	0.8655
Rolling 1-min - Sequential 2-min	266.6472	0.0000	—	—	—	—	0.2176	0.0010
Rolling 2-min - Rolling 3-min	70.3737	0.6135	1.7313	0.1411	1.3552	0.0001	0.0601	0.9014
Rolling 2-min - Rolling 5-min	125.2841	0.0465	—	—	—	—	0.0928	0.5404
Rolling 2-min - Segmented	-109.4113	0.3087	-3.0381	0.0013	-0.8740	0.0752	-0.0712	0.6134
Rolling 2-min - Sequential 1-min	-55.1757	0.8316	-2.2163	0.0292	-0.0429	0.9998	-0.0587	0.9106
Rolling 2-min - Sequential 2-min	92.2842	0.2858	—	—	—	—	0.0942	0.5225
Rolling 3-min - Rolling 5-min	54.9104	0.8351	—	—	—	—	0.0328	0.9952
Rolling 3-min - Segmented	-179.7850	0.0033	-4.7695	0.0000	-2.2291	0.0000	-0.1312	0.0707
Rolling 3-min - Sequential 1-min	-125.5494	0.0456	-3.9476	0.0000	-1.3981	0.0000	-0.1188	0.2435
Rolling 3-min - Sequential 2-min	21.9105	0.9983	—	—	—	—	0.0341	0.9940
Rolling 5-min - Segmented	-234.6954	0.0000	—	—	—	—	-0.1640	0.0115
Rolling 5-min - Sequential 1-min	-180.4598	0.0006	—	—	—	—	-0.1516	0.0570
Rolling 5-min - Sequential 2-min	-32.9999	0.9843	—	—	—	—	0.0014	1.0000
Segmented - Sequential 1-min	54.2356	0.9783	0.8218	0.8385	0.8311	0.1094	0.0124	0.9978
Segmented - Sequential 2-min	201.6955	0.0005	—	—	—	—	0.1654	0.0106
Sequential 1-min - Sequential 2-min	147.4599	0.0095	—	—	—	—	0.1529	0.0531

Table 3-1 **Shorter regression window widths yielded higher MMR estimates in all species. Relative difference (mg O_2 h^{-1}) in mean standardized MMR estimates between compared models with associated *P*-values indicating significance level of comparison (left-most columns). Relative difference in regression slope estimates for each model for California Horn Shark MMR and body mass are shown in the right-most columns (and see Fig. 3-4).**

3.4.2. How does timepoint of the MMR window vary?

MMR occurred more than two minutes after an individual was placed in the respirometer chamber in 77%, 86%, 63%, and 85% of the California Horn Shark, Gray Smoothhound, Rainbow Trout, and Atlantic Salmon individuals, respectively, with the latest window occurring in a California Horn Shark after 11.5 minutes (Fig. 3-3). However, 64% of shark MMR windows occurred within the first five min. There was no consistent pattern of variation in window timepoint and no significant differences between window timepoint means across models ($P > 0.14$ in all cases).

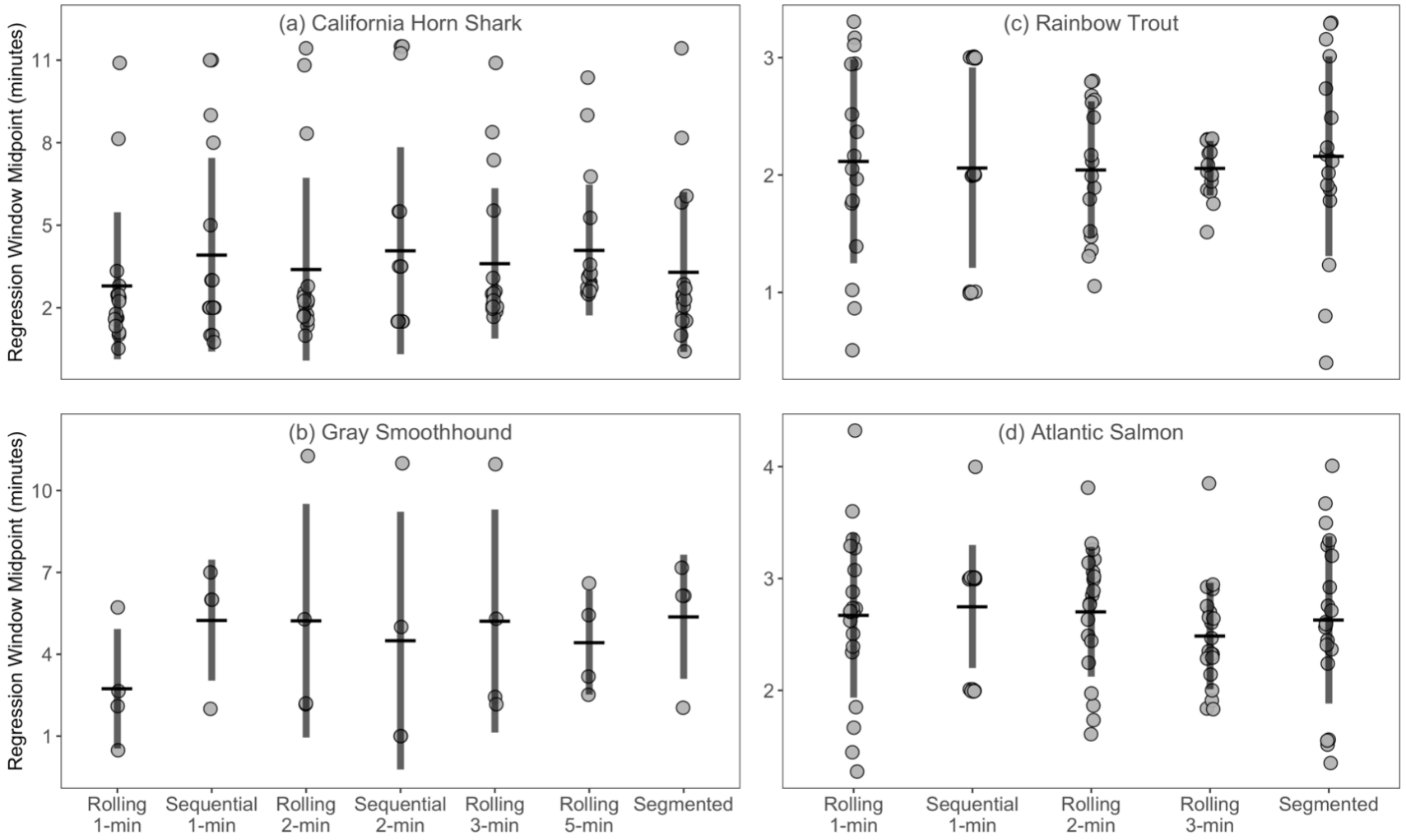
(a) California Horn Shark
(c) Rainbow Trout
(b) Gray Smoothhound
(d) Atlantic Salmon
Regression Window Midpoint (minutes)
Regression Window Midpoint (minutes)
Rolling 1-min
Sequential 1-min
Rolling 2-min
Sequential 2-min
Rolling 3-min
Rolling 5-min
Segmented
Rolling 1-min
Sequential 1-min
Rolling 2-min
Rolling 3-min
Segmented

Figure 3-3 **The timepoint of the MMR regression window within the oxygen depletion trace varied within species but not significantly across models. The timepoint is estimated as the midpoint of the MMR regression window for each model for each individual, measured from when the individual was placed in the respirometer to the midpoint of the MMR regression window. Mean window midpoint is plotted for each model for each species, ± SD.**

3.4.3. Does choice of window width and model affect the scaling of MMR and body mass?

The choice of statistical model had a significant effect on the scaling relationship between MMR and body mass (Table 3-1, Fig.3-4). One-min window rolling regression estimates produced the steepest slope and a relatively wide confidence interval (CI) (1.24 ± 0.11 95% CI). Larger window widths resulted in lower estimated slope values; however, this did not significantly reduce confidence intervals (Fig. 3-4a). The 2-min window rolling regression model MMR estimates resulted in the regression slope estimate with the narrowest confidence interval (1.12 ± 0.07 95% CI). (Fig. 3-4a).

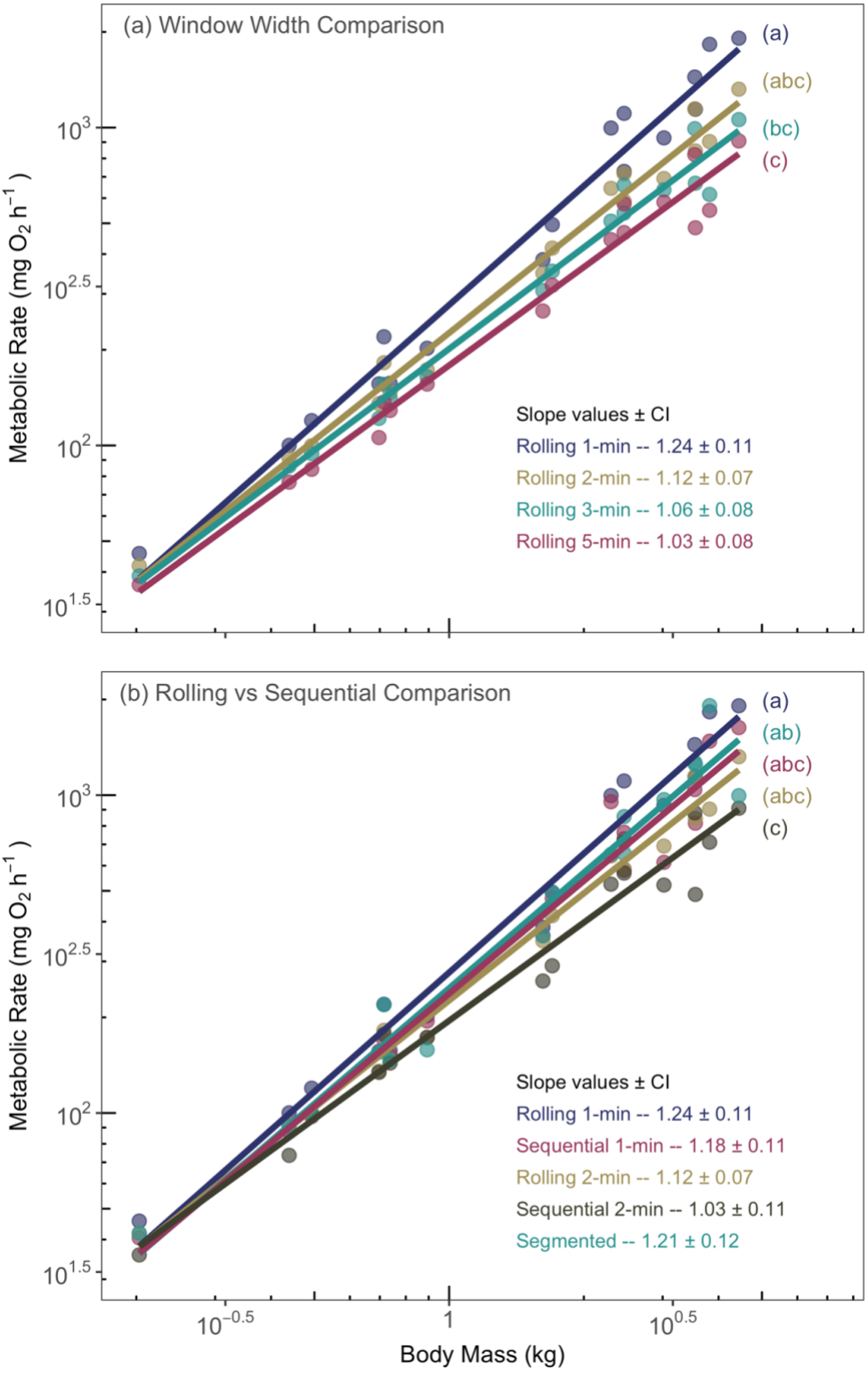
(a) Window Width Comparison
(a)
(abc)
(bc)
(c)
Slope values ± CI
Rolling 1-min -- 1.24 ± 0.11
Rolling 2-min -- 1.12 ± 0.07
Rolling 3-min -- 1.06 ± 0.08
Rolling 5-min -- 1.03 ± 0.08
Metabolic Rate (mg O2 h-1)
10^3
10^2.5
10^2
10^1.5
(b) Rolling vs Sequential Comparison
(a)
(ab)
(abc)
(abc)
(c)
Slope values ± CI
Rolling 1-min -- 1.24 ± 0.11
Sequential 1-min -- 1.18 ± 0.11
Rolling 2-min -- 1.12 ± 0.07
Sequential 2-min -- 1.03 ± 0.11
Segmented -- 1.21 ± 0.12
Metabolic Rate (mg O2 h-1)
10^3
10^2.5
10^2
10^1.5
10^-0.5
1
10^0.5
Body Mass (kg)

Figure 3-4 **Estimates of absolute MMR plotted as a function of body mass on a log-log scale for California Horn Shark for each of the four rolling regression models (a), and rolling regression models with their corresponding window width sequential regression models and the segmented model (b). Slope estimates decreased as window width used to generate estimates increased, and rolling regression slope estimates were higher than their corresponding sequential regression slope estimates. Slope estimates are reported ± 95% confidence intervals. Letters indicate a difference between slope estimates for compared models using a significance level of $P < 0.05$ (and see Table 3-1).**

3.5. Discussion

Across four species of varying activity level and body mass, we find that (1) smaller regression windows yielded higher estimates of MMR, (2) MMR was best estimated using a rolling regression model with a 1- to 2-min window, and (3) the time-point at which MMR typically occurs is at least two minutes into the oxygen depletion trace and, hence, may be missed with certain statistical methods or improper experimental design. This study highlights the necessity of including thorough and detailed statistical methods in the design of respirometry experiments and cautions against directly comparing estimates made with extremely disparate methods. Here, we outline the key considerations in applying these findings in the analysis of fish respirometry data.

3.5.1. Choosing a window width

In all cases, MMR estimates were sensitive to the window width used in analysis. All statistical models required at least a minimum window width be chosen in order to estimate MMR and this choice remains somewhat subjective. If too short a window is used, MMR may be overestimated due to spurious non-oxygen consumption variance in the system. However, attempting to guard against this with too long of a window width may unnecessarily underestimate MMR without adding significant variance-handling benefits. At a minimum, raw traces of oxygen depletion over time should be visually checked to get a sense for how reasonable each potential window width and corresponding MMR estimate may be. Traces that contain obvious non-linear sections, such as the example California Horn Shark trace in Fig. 3-1c-f, may require longer window widths compared to more linear traces. As an additional test, when California Horn Shark data were regressed as a function of body mass, the 2-min window rolling regression estimates produced the smallest confidence interval around the slope estimate of all our tested models (slope = 1.12 ± 0.07) (Fig. 3-4). This suggests that this slightly longer window width may be more appropriate for this data set to account for and reduce the influence of higher system variance at larger body masses and respirometry chamber sizes. However, we cannot exclude the possibility that the true estimates of MMR are highly variable across individuals. At this time, we recommend using the same window width across all individuals in a study for consistency.

While we found a negative relationship between MMR estimate and widow width in all species, this effect was considerably weaker in the small salmonids than the much larger sharks (Fig. 3-2 a, c, e, f). This suggests that estimates made using different, but similar, window widths may be more comparable across studies in which relatively small body masses and chambers were used, while studies utilizing different window widths for larger animals and larger chambers may be less comparable. During analysis, multiple window widths should be compared before deciding on the best width for the experimental system, as we have done here. Methods to estimate system-specific regression window widths show promise, however, our test of the signal-to-noise ratio method showed that this method was unable to differentiate between experimental systems to produce a reliable regression window width (see Appendix B) (Zhang et al., 2019).

3.5.2. Choosing a statistical model

The rolling regression model proved to be the most versatile and precise method for estimating MMR and worked well across all species and experimental systems. Its overlapping intervals mean this model has the resolution to test every possible regression within the oxygen depletion dataset, greatly reducing the chance of missing the MMR window and making it unnecessary to select a lag period to remove from the beginning of the trace. Statistical software packages such as *respR* make it simple to implement this model on raw data output from a wide variety of oxygen sensing equipment and improve reproducibility across studies (Harianto et al., 2019). In contrast, the sequential regression model performed poorly. By placing the regression windows end-to-end, the low resolution of these models consistently underestimated MMR compared to rolling regression models using the same window width (Fig. 3-1b, 3-2, Table 3-1). Specifically, sequential regression may miss the true MMR window if it occurs partially across two successive regression widows. For example, for a 3-min long MMR trace, a sequential regression model can only produce three 1-min regression estimates while rolling regression would produce 121 estimates, providing a view of oxygen consumption rate at every single timepoint during the oxygen depletion trace. Similarly, the segmented regression model was unable to consistently produce reasonable MMR estimates across individuals, as seen through the large variation in

estimates across individuals in comparison to other models (Fig. 3-2, B-1). Selecting a minimum allowable regression window width for the segmented regression was highly subjective, and in one case, allowing a 41 s rather than a 45 s window would have doubled the resulting MMR estimate (Fig. B-1a). Spurious changes in oxygen consumption rate, especially in the larger respirometer chambers, lead to the estimation of breakpoints at timepoints where there likely wasn't a true significant change in the rate of oxygen consumption (Fig. 3-1e). Thus, we recommend rolling regression be used to estimate MMR in aquatic systems.

3.5.3. Choosing a measurement period

Respirometry experiments are often designed to use short, 3-to 5-min measurement periods under the assumption that individuals will be maximumly aerobic during and immediately following strenuous exercise (Brett, 1964; Norin and Clark, 2016; Rummer et al., 2016). Longer measurement periods may also not be feasible for species with high metabolic rates that rapidly deplete available oxygen within the respirometer (Svendsen et al., 2016b). While MMR occurred immediately in most individuals, there were many instances where it occurred after a considerable delay and would have been missed if a shorter measurement period was used (Fig. 3-3). An extreme case of delayed MMR was found by Clark et al. (2012) in Coho Salmon (*Oncorhynchus kisutch*), where MMR peaked up to five hours after exhaustive exercise. To have the best chance of catching the MMR window, an effort should be made to use the longest measurement period possible for the tested species and experimental system.

3.5.4. Conclusions

When plotted against body mass on a log-log scale, the MMR estimates made with each model for California Horn Shark revealed a pattern of decreasing slope coefficients with increasing regression window widths (Fig. 3-4). This pattern suggests that MMR estimates may not be comparable across studies where significantly different statistical methods were used to generate them, such as 1 *vs.* 5-min regression window widths, especially in larger individuals. However, more work is needed to investigate the consequences of grouping estimates made with potentially disparate statistical methods. Glazier (2005) highlighted that standard MMR estimates for the same species can vary between studies but that it is unclear how much of this is the result of variation across

individuals or variation in study design. Because each of our models was tested on the same raw data, we have strong support that the statistical method itself is likely the cause of the observed variation in estimates in many cases. We suggest MMR statistical analysis method be considered, in addition to the standard practice of accounting for temperature and experimental protocol, when collating data in future meta-analyses (e.g. Killen et al., 2016).

Despite the considerable increase in appreciation for metabolic ecology and the experimental methods required to estimate metabolic rate, the choice of statistical methods has remained largely unstandardized. The implications are far-reaching, from the quality of empirical studies and theoretical models to the comparability of results across species and metabolic ecology's potential as a predictive tool (Deutch et al., 2015; Glazier, 2009) Additionally, precise estimates of MMR are crucial to understanding species' response to thermal extremes through the lens of aerobic scope, defined as an animal's capacity for activity above rest (Farrell, 2016).

We strongly encourage the use of systematic testing of MMR window-width as outlined in this paper and the use of rolling regression models in future MMR studies. In addition, authors should report their analytical choices by following principles of reproducible code and data archiving so that future meta-analyses can more accurately assess interspecific relationships and produce reliable results (Croucher et al., 2017).

3.6. References

Auer, S. K., Salin, K., Anderson, G. J., & Metcalfe, N. B. (2018). Individuals exhibit consistent differences in their metabolic rates across changing thermal conditions. *Comparative Biochemistry and Physiology -Part A : Molecular and Integrative Physiology*, *217*, 1–6. doi:10.1016/j.cbpa.2017.11.021

Barneche, D. R., Kulbicki, M., Floeter, S. R., Friedlander, A. M., Maina, J., & Allen, A. P. (2014). Scaling metabolism from individuals to reef-fish communities at broad spatial scales. *Ecology Letters*, *17*(9), 1067–1076. doi:10.1111/ele.12309

Bates, D., Mächler, M., Bolker, B. M., & Walker, S. C. (2015). Fitting linear mixed-effects models using lme4. *Journal of Statistical Software*, *67*(1). doi:10.18637/jss.v067.i01

Brett, J. R. (1964). The respiratory metabolism and swimming performance of young sockeye salmon. *Journal of Visual Languages & Computing*, *5*(21), 55.

Brown, J. H., Gillooly, J. F., Allen, A. P., Savage, V. M., & West, G. B. (2004). Toward a metabolic theory of ecology. *Ecology*, *85*(7), 1771–1789. doi:doi.org/10.1890/03-9000

Cech Jr, J. J., & Brauner, C. J. (2011). *Techniques in Whole Animal Respiratory Physiology*. *Encyclopedia of Fish Physiology: From Genome to Environment* (Vol. 2). Elsevier Inc. doi:10.1016/B978-0-1237-4553-8.00128-3

Cheung, W. W. L., Sarmiento, J. L., Dunne, J., Frölicher, T. L., Lam, V. W. Y., Palomares, M. L. D., … Pauly, D. (2013). Shrinking of fishes exacerbates impacts of global ocean changes on marine ecosystems. *Nature Climate Change*, *3*(3), 254–258. doi:10.1038/nclimate1691

Clark, T. D., Sandblom, E., & Jutfelt, F. (2013). Aerobic scope measurements of fishes in an era of climate change: respirometry, relevance and recommendations. *Journal of Experimental Biology*, *216*(15), 2771–2782. doi:10.1242/jeb.084251

Croucher, M., Graham, L., James, T., Krystalli, A., & Michonneau, F. (2017). *A Guide to Reproducible Code in Ecology and Evolution*. *BES Guides to Better Science*.

Deutch, C., Ferrel, A., Seibel, B., Pörtner, H. O., & Huey, R. B. (2015). Climate change tightens a metabolic constraint on marine habitats. *Science*, *348*(6239), 1132–1136.

Farrell, A. P. (2016). Pragmatic perspective on aerobic scope: Peaking, plummeting, pejus and apportioning. *Journal of Fish Biology*, *88*(1), 322–343. doi:10.1111/jfb.12789

Glazier, D. S. (2005). Beyond the '3/4-power law': Variation in the intra- and interspecific scaling of metabolic rate in animals. *Biological Reviews of the Cambridge Philosophical Society*, *80*(4), 611–662. doi:10.1017/S1464793105006834

Glazier, D. S. (2009). Activity affects intraspecific body-size scaling of metabolic rate in ectothermic animals. *Journal of Comparative Physiology B: Biochemical, Systemic, and Environmental Physiology*, *179*(7), 821–82. doi:10.1007/s00360-009-0363-3

Harianto, J., Carey, N., & Byrne, M. (2019). respR—An R package for the manipulation and analysis of respirometry data. *Methods in Ecology and Evolution*, *10*(6), 1–9. doi:10.1111/2041-210X.13162

Killen, S. S., Costa, I., Brown, J. A., & Gamperl, A. K. (2007). Little left in the tank: Metabolic scaling in marine teleosts and its implications for aerobic scope. *Proceedings of the Royal Society B: Biological Sciences*, *274*(1608), 431–438. doi:10.1098/rspb.2006.3741

Killen, S. S., Glazier, D. S., Rezende, E. L., Clark, T. D., Atkinson, D., Willener, A. S. T., & Halsey, L. G. (2016). Ecological Influences and Morphological Correlates of Resting and Maximal Metabolic Rates across Teleost Fish Species. *The American Naturalist*, *187*(5), 592–606. doi:10.1086/685893

Muggeo, V. M. R. (2003). Estimating regression models with unknown break-points. *Statistics in Medicine*, *22*(19), 3055–3071. doi:10.1002/sim.1545

Muggeo, V. M. R. (2008). Modeling temperature effects on mortality: Multiple segmented relationships with common break points. *Biostatistics*, *9*(4), 613–620. doi:10.1093/biostatistics/kxm057

Norin, T., & Clark, T. D. (2016). Measurement and relevance of maximum metabolic rate in fishes. *Journal of Fish Biology*, *88*(1), 122–151. doi:10.1111/jfb.12796

Norin, T., Malte, H., & Clark, T. D. (2016). Differential plasticity of metabolic rate phenotypes in a tropical fish facing environmental change. *Functional Ecology*, *30*(3), 369–378. doi:10.1111/1365-2435.12503

Payne, N. L., Snelling, E. P., Fitzpatrick, R., Seymour, J., Courtney, R., Barnett, A., … Semmens, J. M. (2015). A new method for resolving uncertainty of energy requirements in large water breathers: The 'mega-flume' seagoing swim-tunnel respirometer. *Methods in Ecology and Evolution*, *6*(6), 668–677. doi:10.1111/2041-210X.12358

Pörtner, H. O., Bock, C., & Mark, F. C. (2017). Oxygen- & capacity-limited thermal tolerance: Bridging ecology & physiology. *Journal of Experimental Biology*, *220*(15), 2685–2696. doi:10.1242/jeb.134585

Reemeyer, J. E., & Rees, B. B. (2019). Standardizing the determination and interpretation of Pcrit in fishes. *Journal of Experimental Biology*, *222*(18). doi:10.1242/jeb.210633

Roche, D. G., Binning, S. A., Bosiger, Y., Johansen, J. L., & Rummer, J. L. (2013). Finding the best estimates of metabolic rates in a coral reef fish. *Journal of Experimental Biology*, *216*(11), 2103–2110. doi:10.1242/jeb.082925

Rummer, J. L., Binning, S. A., Roche, D. G., & Johansen, J. L. (2016). Methods matter: Considering locomotory mode and respirometry technique when estimating metabolic rates of fishes. *Conservation Physiology*, *4*(1). doi:10.1093/conphys/cow008

Slesinger, E., Andres, A., Young, R., Seibel, B., Saba, V., Phelan, B., … Saba, G. (2019). The effect of ocean warming on black sea bass (*Centropristis striata*) aerobic scope and hypoxia tolerance. *PLoS ONE*, *14*(6), 1–22. doi:10.1371/journal.pone.0218390

Svendsen, M. B. S., Bushnell, P. G., & Steffensen, J. F. (2016). Design and setup of intermittent-flow respirometry system for aquatic organisms. *Journal of Fish Biology*, *88*(1), 26–50. doi:10.1111/jfb.12797

Tirsgaard, B., Behrens, J. W., & Steffensen, J. F. (2015). The effect of temperature and body size on metabolic scope of activity in juvenile Atlantic cod *Gadus morhua* L. *Comparative Biochemistry and Physiology -Part A : Molecular and Integrative Physiology*, *179*, 89–94. doi:10.1016/j.cbpa.2014.09.033

White, C. R., & Kearney, M. R. (2013). Determinants of inter-specific variation in basal metabolic rate. *Journal of Comparative Physiology B: Biochemical, Systemic, and Environmental Physiology*, *183*(1), 1–26. doi:10.1007/s00360-012-0676-5

Xiao, X., White, E., Hooten, M., & Durham, S. (2011). On the use of log-transformation vs. nonlinear regression for analyzing biological power-laws. *Ecology*, *92*(10), 110606103516051. doi:10.1890/11-0538.1

Závorka, L., Brijs, J., Wengström, N., Wallerius, M. L., Näslund, J., Koeck, B., … Cucherousset, J. (2018). Laboratory captivity can affect scores of metabolic rates and activity in wild brown trout. *Journal of Zoology*, *307*, 249–255. doi:10.1111/jzo.12642

Zhang, Y., Gilbert, M. J. H., & Farrell, A. P. (2019). Finding the peak of dynamic oxygen uptake during fatiguing exercise in fish. *The Journal of Experimental Biology*, *222*(12), 1–8. doi:10.1242/jeb.196568

Zhang, Y., Gilbert, M. J. H., & Farrell, A. P. (2020). Measuring maximum oxygen uptake with an incremental swimming test and by chasing rainbow trout to exhaustion inside a respirometry chamber yield the same results. *Journal of Fish Biology*, (97), 1–11. doi:10.1111/jfb.14311

Zhang, Y., Timmerhaus, G., Anttila, K., Mauduit, F., Jørgensen, S. M., Kristensen, T., … Farrell, A. P. (2016). Domestication compromises athleticism and respiratory plasticity in response to aerobic exercise training in Atlantic salmon (*Salmo salar*). *Aquaculture*, *463*, 79–88. doi:10.1016/j.aquaculture.2016.05.015

Chapter 4. **Conclusion**

In this thesis, I used both a lab experiment and collated data to test two of the fundamental tools with which we examine metabolic rate: The scaling of gill surface area and metabolic rate with body mass within species, and the statistical analysis of maximum metabolic rate data for fishes. Here, I overview the key findings of each data chapter, their implications, caveats, and future directions for this research.

In chapter 2, I used California Horn Shark as a study species to explore gill area in relation to the intraspecific scaling of resting and maximal metabolic rate and body mass. I asked if metabolic level (i.e., resting or maximum metabolic rate) was correlated with variation in the slope of metabolic rate and body mass, and if gill area was related to this variation in slope between metabolic levels. I found that the allometric slope of maximum metabolic rate (MMR, 1.079 ± 0.044 95% CI) was significantly steeper than the slope of resting metabolic rate (RMR, 0.971 ± 0.064) and gill area (0.888 ± 0.077). However, I found that a broken-stick regression better explained the relationship between gill area and body mass than a linear model, where the slope of gill area across adolescents and adults (at ≥ 0.203 kg body mass = 1.014 ± 0.151) was not significantly different from the slope of either MMR or RMR (Figs. 2-1, 2-3).

Firstly, these results do not support the hypothesis that oxygen demand is limited by supply in California Horn Shark, which is an inactive, benthic species. Metabolic rate at both resting and maximum metabolic levels scaled isometrically or above, which – at first glance -– is inconsistent with the surface area-to-volume constraints of the gill oxygen limitation theory (Pauly, 2010; Pauly and Cheung, 2017). But inactive species that put little pressure on their surface areas are hypothesised to have metabolic rate scaling exponents that are more similar to body mass scaling (Glazier 2005; Killen et al., 2010). This is the pattern shown here in California Horn Shark, an inactive benthic species which spends a considerable amount of time at rest (Meese and Lowe, 2020). Further, I found that metabolic level (RMR vs MMR) influences how metabolic rate scales with body mass (Glazier, 2005). Therefore, this work supports the hypothesis that activity level and metabolic level are partly responsible for the variation in the slope of metabolic rate and body mass across species and suggests that this variation is not

simply statistical noise around a mean value. However, these results are one test within one species. Though they contribute to the body of work supporting this hypothesis, further analyses using more diverse species are required to better establish the details of the relationship between metabolic level and the allometric scaling of metabolic rate. For example, Rubalcaba et al. (2020) used data from 286 species of fishes to show that MMR may be more constrained by oxygen limitation than RMR, potentially leading to a higher sensitivity to oxygen availability in larger, warmer, active fish species. However, my results here demonstrate that there may be significant variation in ontogenetic allometries (and the resulting mean estimates) depending on the body-size range used, and we must establish whether this may then affect the meta-analyses which collate these estimates. Future work should explore the effect of ontogenetic size range on mean metabolic rate estimate to determine if there is a minimum acceptable size range required for reliably generating these mean estimates.

The allometric scaling of gill area in relation to metabolic rate shown here suggests that metabolic rate is not limited by surface area-to-volume constraints on oxygen diffusion, at least at the gills. Gill area, a surface, was able to scale isometrically with body mass, a volume, when examined with the broken stick regression model (Fig. 2-1). In an inactive species like the California Horn Shark, metabolic demands are relatively low, and possessing enough gill area to meet those demands likely does not require the animal to push the limits of available space in its head (Wegner, 2016). Therefore, it is not too surprising that we see isometric scaling of metabolic rate and of gill area after the juvenile life stage and through adulthood (Fig. 2-1). In contrast, we may see a different scaling pattern in a relatively active fish species. In order to match high metabolic needs, the gills may be at their physiological limit in terms of surface area crammed into the head, and we may see a pattern of shallower scaling exponents for both gill area and metabolic rate (Hughes, 1984). However, there have yet to be any studies which use a complete ontogeny to examine the allometric scaling of gill area, maximum and resting metabolic rates in an active fish species, preventing us from confirming this shallower slope prediction.

The physiological roles gills play in addition to gas exchange surfaces support a change in slope with developmental stage. In addition to oxygen diffusion, the gills also help regulate the exchange of ions and waste products with the surrounding environment, a metabolically costly exercise (Ern et al, 2014). If gill area scales linearly

across the full body size range, the excess gill area necessary to support the steep scaling exponents for MMR and RMR found here would require a significant energetic investment (Ern et al. 2014). It is therefore unlikely that gill area scales consistently across body mass, and I speculate that adding more individuals smaller than 200 grams would support the hypothesis of a change in gill area slope with developmental stage. Additionally, elasmobranchs hatch as fully formed juveniles with adult-like body morphology, thus limiting the amount of gas exchange which can occur over their skin while still inside the egg case (Rodda and Seymour, 2008; Toulmond, 1982). In contrast to bony fishes, egg-laying elasmobranchs probably hatch with excess gill area relative to their metabolic demands, likely due to residual compensation for a lack of cutaneous gas exchange inside the egg case (Fig. 2-3). As body mass increases, the ratio of gill area to metabolic rate may balance out as oxygen supply is aligned with oxygen demand. However, more paired estimates of metabolic rate and gill area in other oviparous elasmobranch species are necessary before we can conclude that a shift in the scaling of gill area relative to metabolic rate is not just an anomaly found here.

In chapter 3, I tested three statistical models for estimating MMR in two shark and two salmonid species. This research emerged as a necessary part of my California Horn Shark experiment, as my literature searches failed to turn up a clear explanation of how to approach the analysis of MMR data for aquatic respirometry. Oxygen consumption over time is used as a proxy for metabolic rate, and MMR is defined as an unsustainably high level of activity (Norin and Clark 2016). Thus, we expect MMR to occur over a relatively short period of time, yet too short a regression window significantly increases the risk of overestimating MMR. I found that a rolling regression model with a 1-to 2-minute regression window was the most simple, versatile, and objective model for estimating MMR across my four tested species. However, I was unable to establish a definitive method for selecting a window width. As part of the development of this project, I used simulated data to test a model for estimating a respirometer-specific window width (Appendix B) (Zhang et al., 2019). Unfortunately, the model was unable to differentiate between simulated experimental systems and was sensitive to the sample size used in analysis (Fig. B-3). I recommended that the variance around mean MMR estimates at each window width be compared to help select an appropriate window width, but again, more data for more diverse species is needed to develop a precise selection method. This is something I would like to explore further in

the future. MMR is increasingly being studied and the data exists, just waiting for someone to collate and analyze it.

With this thesis, I hoped to draw attention to the need to understand the fundamentals of scaling and experimental methods before we can produce informative meta-analyses and apply metabolic theory. Because ecosystems are so complex, I envision that metabolic theory will be applied to smaller groups of related species individually and then those results will be scrutinized to form a larger, more cohesive understanding of the ecosystem in question. We see so much variation in metabolic rate across species that it will be extremely difficult, and perhaps not very useful, to search for and apply a single scaling coefficient in all instances (Bokma, 2004). Thus, studies which aim to find the correlates of this variation likely have a better chance of contributing to our metabolic ecology toolbox. A significant part of this equation is the estimates of metabolic rate themselves. While disparate methods across studies may not make a significant difference when the focus is on the individual study itself, we may run into problems when we then try to compare those data to other work and across species. This seems obvious, which is why it was so surprising to find so little discussion of MMR statistical analysis methods in the literature. In my third chapter I was only able to study four species, California Horn Shark, Gray Smoothhound, Rainbow Trout and Atlantic Salmon, but the results support other work highlighting that method may have a significant on MMR estimate (Roche et al., 2013; Rummer et al., 2016). Because of limited body size ranges, I was only able to test the effect of MMR analysis method on the scaling of metabolic rate and body mass in California Horn Shark. I found that method significantly affected the allometric slope of MMR, and future work should investigate if this occurs in other species. Importantly, the predictive power of metabolic theory relies on the quality of the data used in models. A better understanding of the physiological underpinnings of the variation we see in metabolic rate, and better standardization of the methods used to study it, will help ensure the predictive capacity of metabolic theory in future studies.

4.1. References

Bokma, A. F. (2004). Evidence against Universal Metabolic Allometry. *Funct. Ecol.* 18, 184–187.

Ern, R., Huong, D. T. T., Cong, N. V., Bayley, M. and Wang, T. (2014). Effect of salinity on oxygen consumption in fishes: A review. *J. Fish Biol.* 84, 1210–1220.

Glazier, D. S. (2005). Beyond the “3/4-power law”: Variation in the intra- and interspecific scaling of metabolic rate in animals. *Biol. Rev. Camb. Philos. Soc.* 80, 611–662.

Killen, S. S., Atkinson, D. and Glazier, D. S. (2010). The intraspecific scaling of metabolic rate with body mass in fishes depends on lifestyle and temperature. *Ecol. Lett*. 13, 184–193.

Lefevre, S., McKenzie, D. J. and Nilsson, G. E. (2017). Models projecting the fate of fish populations under climate change need to be based on valid physiological mechanisms. *Glob. Chang. Biol*. 23, 3449–3459.

Meese, E. N. and Lowe, C. G. (2020). Active acoustic telemetry tracking and tri- axial accelerometers reveal fine-scale movement strategies of a non-obligate ram ventilator. *Mov. Ecol.* 8, 1–17.

Norin, T. and Clark, T. D. (2016). Measurement and relevance of maximum metabolic rate in fishes. *J. Fish Biol.* 88, 122–151.

Roche, D. G., Binning, S. A., Bosiger, Y., Johansen, J. L. and Rummer, J. L. (2013). Finding the best estimates of metabolic rates in a coral reef fish. *J. Exp. Biol.* 216, 2103–2110.

Rodda, K. R. and Seymour, R. S. (2008). Functional morphology of embryonic development in the Port Jackson shark *Heterodontus portusjacksoni* (Meyer). *J. Fish Biol.* 72, 961–984.

Rubalcaba, J. G., Verberk, W. C. E. P., Hendriks, A. J., Saris, B. and Woods, H. A. (2020). Oxygen limitation may affect the temperature and size dependence of metabolism in aquatic ectotherms. *Proc. Natl. Acad. Sci*. 117, 31963–31968.

Rummer, J. L., Binning, S. A., Roche, D. G. and Johansen, J. L. (2016). Methods matter: Considering locomotory mode and respirometry technique when estimating metabolic rates of fishes. *Conserv. Physiol.* 4, 1–13.

Toulmond, A. (1982). Cutaneous O2 and CO2 exchanges in the dogfish, *Scyliorhinus canicula. Respir. Physiol.* 48, 169–181.

Wegner, N. C. (2016). Elasmobranch Gill Structure. In Physiology of Elasmobranch Fishes: Structure and Interaction with Environment. (ed. Shadwick, R. E., Farrell, A. P., and Brauner, C. J.), pp. 101–151. New York City, NY: Academic Press.

Zhang, Y., Gilbert, M. J. H. and Farrell, A. P. (2019). Finding the peak of dynamic oxygen uptake during fatiguing exercise in fish. *J. Exp. Biol.* 222, 1–8.

Appendix A.

Supplementary material for Chapter 2

A.1.1 Comparison of MMR experimental methods

To determine which MMR method produced the highest estimates, we compared mean standardized MMR estimates made with each method. Each MMR estimate was standardized to mean body mass for each sample size (1.75 kg) by calculating residual MMR values as the difference between the measured and predicted MMR value according to the relationship between MMR and body mass (MMR = $a\ M^{b}$ where a and b are constants calculated for each MMR method, and M is body mass) (Norin, Malte, & Clark, 2016). Residual values were normally distributed (Shapiro-Wilk, $p > 0.05$) for all MMR estimates. For each individual, we then added the raw residual MMR value (positive or negative) to the predicted MMR value at the mean body mass to standardize absolute MMR to the mean body mass. We then fit a linear mixed effects model with standardized MMR estimate (MMR *chase* and MMR *chase + air*) as a function of MMR method name with individual identity as a random effect (Bates et al., 2015). We used a general linear hypothesis test to compare between mean estimates for each MMR method (Hothorn et al., 2008). Further analysis used only estimates produced using the MMR method found to consistently produce the highest estimates.

A.1.2 MMR method comparison results

Standardized estimates made with the MMR chase method were higher than those made with the MMR chase + air method in 16 out of the 19 Horn shark, where mean MMR chase was 8% higher than mean MR chase + air. However, this difference was not significant (LMM, $F_{2, 17} = 2.68$, $P = 0.101$). In contrast, the slope of MMR *chase+air* was slightly greater than that of MMR *chase*, but this also did not differ significantly (Fig. 1, 2).

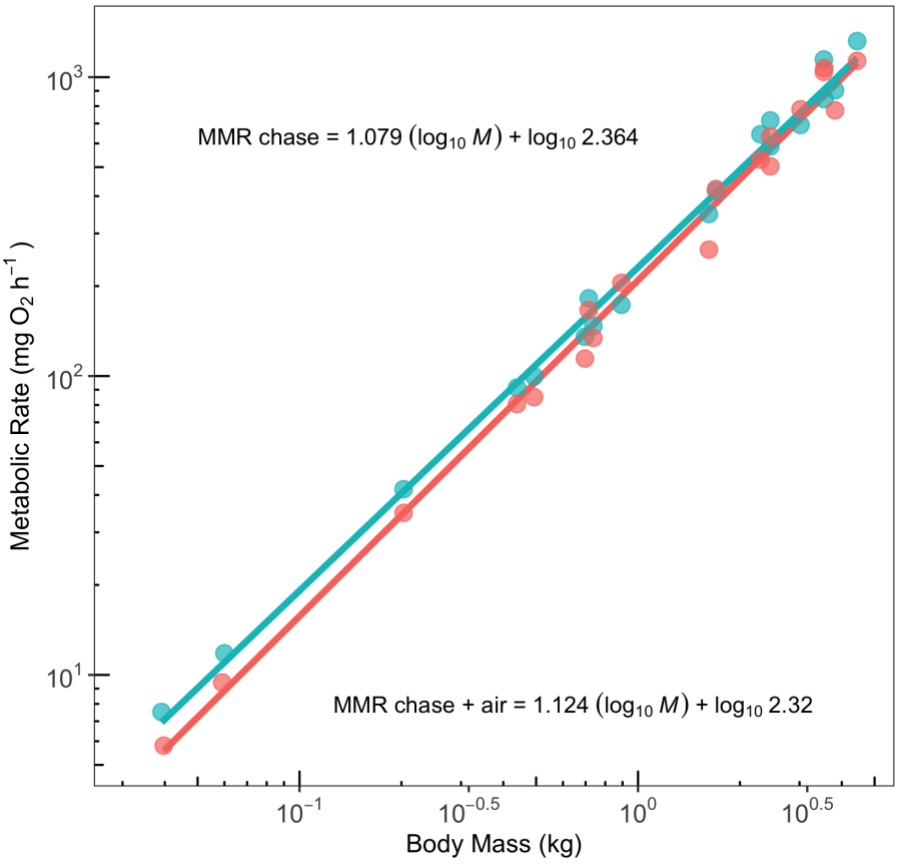

Figure A-1 Scaling of maximum metabolic rate (MMR) as a function of body mass for each experimental method, *chase* or *chase* + *air*.

Because horn shark are slow swimmers, we hypothesized that using a period of air exposure would be necessary to fully exhaust the individuals and produce sufficiently high estimates of MMR (Schwieterman et al., 2019). In contrast to previous work, adding a period of air exposure after an exhaustive chase produced slightly lower estimates of MMR compared to the chase-only method, though this difference was not significant (Roche et al., 2013, Rummer et al. 2016). However, there was a larger difference between the experimental methods compared in these other studies than between the methods compared here; we added a period of air exposure to a chase protocol for comparison, while two unique protocols were compared in each of these other studies (Roche et al., 2013, Rummer et al. 2016). The similarity of our protocols may have resulted in the similar estimates we found, but there was a consistent pattern of higher estimates with the MMR chase protocol, suggesting this difference was not an anomaly. It is possible that the stress of air exposure may have caused the animal to widen its recovery window once placed in the respirometer chamber, thus reducing the rate of oxygen consumption and lowering the final MMR estimate. These results suggest that a chase to exhaustion protocol may be sufficient to elicit MMR even in species categorized as weak swimmers, however, they add to the currently mixed evidence surrounding the effect of experimental method on MMR estimate (Killen et al., 2017; Reidy et al., 1995). Caution should be used when comparing estimates made using different experimental methods, and preliminary trials should be run to determine species-specific methods during experiments.

A.2 References

Bates, D., Maechler, M., Bolker, B., Walker, S. (2015). Fitting Linear Mixed Effects Models Using lme4. *Journal of Statistical Software*, 67(1), 1-48. doi:10.18637/jss.v067.i01.

Hothorn, T., Bretz, F. and Westfall P. (2008). Simultaneous Inference in General Parametric Models. *Biometrical Journal* 50(3), 346--363.

Killen, S. S., Norin, T. and Halsey, L. G. (2017). Do method and species lifestyle affect measures of maximum metabolic rate in fishes? *J. Fish Biol.* 90, 1037–1046.

Norin, T., Malte, H. and Clark, T. D. (2016). Differential plasticity of metabolic rate phenotypes in a tropical fish facing environmental change. *Funct. Ecol.* 30, 369–378.

Reidy, S. P., Nelson, J. A., Tang, Y. and Kerr, S. R. (1995). Post-exercise metabolic rate in Atlantic cod and its dependence on the method of exhaustion. *J. Fish Biol.* 47, 377–386.

Roche, D. G., Binning, S. A., Bosiger, Y., Johansen, J. L. and Rummer, J. L. (2013). Finding the best estimates of metabolic rates in a coral reef fish. *J. Exp. Biol.* 216, 2103–2110.

Rummer, J. L., Binning, S. A., Roche, D. G. and Johansen, J. L. (2016). Methods matter: Considering locomotory mode and respirometry technique when estimating metabolic rates of fishes. *Conserv. Physiol.* 4, 1-13

Schwieterman, G.D., Crear, D.P., Anderson, B.N., Lavoie, D.R., Sulikowski, J.A., Bushnell, P.G., Brill, R.W. (2019) Combined Effects of Acute Temperature Change and Elevated pCO2 on the Metabolic Rates and Hypoxia Tolerances of Clearnose Skate (*Rostaraja eglanteria*), Summer Flounder (*Paralichthys dentatus),* and Thorny Skate (*Amblyraja radiata*). *Biology* 8(56) 1-19 doi:10.3390/biology8030056

Appendix B.

Supplementary material for Chapter 3

B.1.1 Animal acquisition

Elasmobranchs were caught as bycatch during yearly gillnet surveys near San Diego, California and by hand using scuba. Rainbow Trout were supplied by Fraser Valley Trout Hatchery Abbotsford, British Columbia (BC), Canada (Freshwater Fisheries Society of BC). All data were collected as part of other ongoing projects at the NOAA Southwest Fisheries Science Center in La Jolla, California and the University of British Columbia in Vancouver, BC.

B.1.2 Collection of oxygen consumption data

All experiments were carried out using a chase-to-exhaustion protocol where each individual was manually chased by hand in a tank large enough to allow unimpeded burst-swimming (Norin & Clark, 2016; Zhang, et al. 2020; Zhang et al., 2016). Once exhausted, the focal individual was immediately transferred from the chase tank to the respirometer chamber (Loligo systems, Tjele, Denmark). This process was practiced and optimized so that transfer time from chase tank to respirometer chamber took less than 20-30 s. Oxygen consumption over time was measured for a minimum of 10 min for Horn Shark and Smoothhound, ending once the dissolved oxygen concentration reached 80%. For Rainbow Trout and Atlantic Salmon, a standard, short measurement period protocol was followed and oxygen consumption was measured over a shorter 3.5-4.5 min period. This corresponds to the closed or measurement period, after which the flush valve was opened to flush the chamber with new, fully oxygenated water during the flush period. Background respiration was measured in empty respirometer chambers immediately before or after an M_{O_2max} trial and was found to be negligible in all cases.

Water was mixed inside the respirometer chamber using a recirculating closed-loop system with a water pump (Eheim, Deizisau, Germany), and a fiber-optic oxygen probe was fixed in the recirculation loop to measure dissolved oxygen once every

second (Svendsen et al., 2016). Horn Shark and Smoothhound respirometry data were collected using Fibox 3 and Fibox 4 oxygen meters and probes (PSt3 Oxygen Dipping Probe, PreSens Precision Sensing GmbH, Germany), and Rainbow Trout and Atlantic Salmon data were collected using Firesting oxygen meters (FSO2-4 optical oxygen and temp meter FireStingO2) and fiber optic probes (Robust Oxygen Probe OXROB10, PyroScience GmbH, Aachen, Germany). All dissolved oxygen measurements were converted to units of mg/L using the *respR* oxygen unit conversion function(Harianto et al., 2019), accounting for temperature and atmospheric pressure. All experiments were carried out on fasted, laboratory acclimated fish. Because fish species varied in size, multiple respirometer chambers were used to appropriately match the chamber volume to each fish's body mass. Teleost experiments were carried out using 2.25-2.26 litre respirometer chambers only. For Horn Shark experiments, the range of chamber sizes was 5.825 litres to 52.5 litres with a mean chamber-to-fish volume ratio of 15.27. For Smoothhounds, the range of chamber sizes was 14.2 litres to 52.5 litres with a mean chamber-to-fish volume ratio of 38.

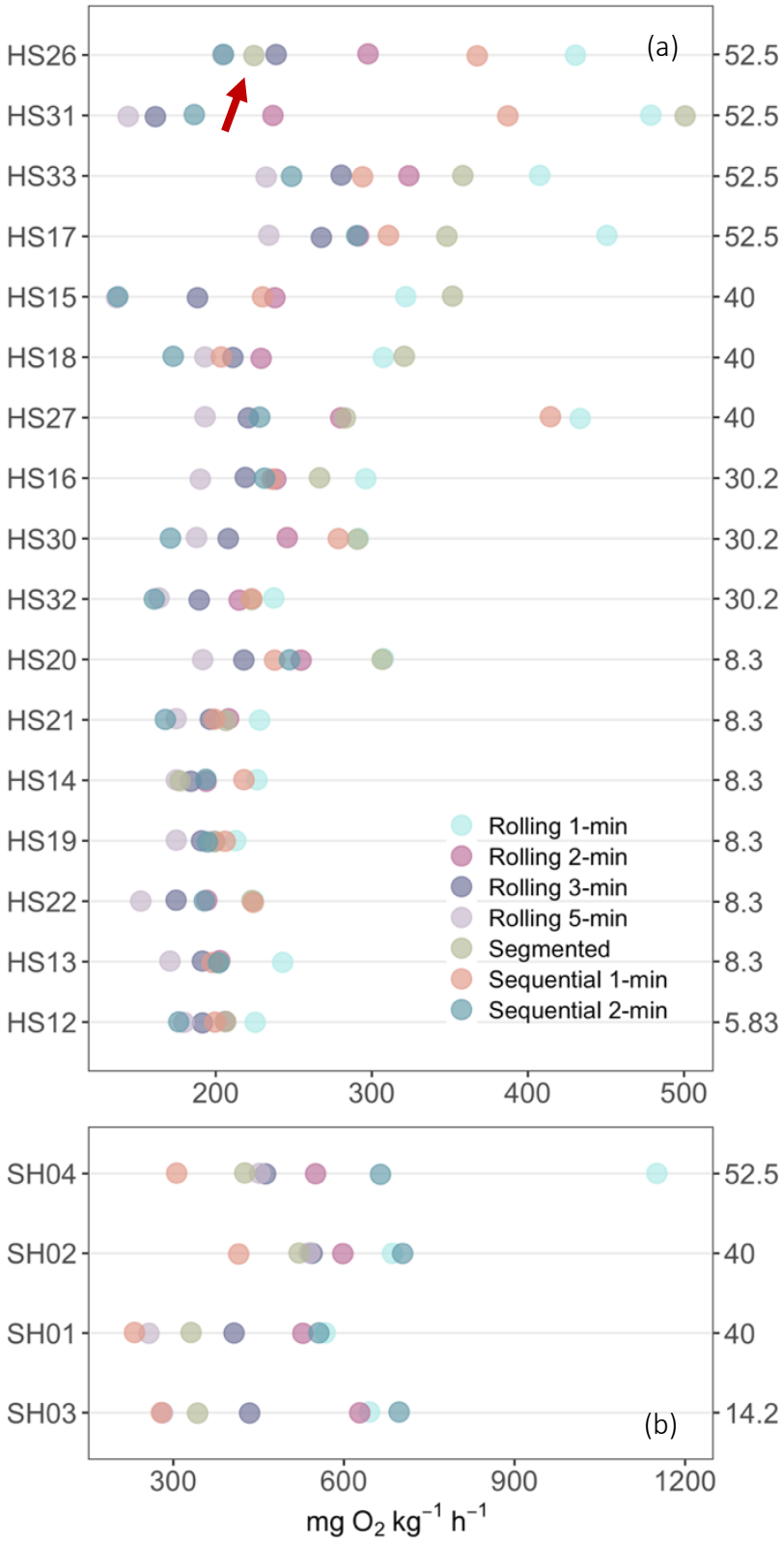
(a)
HS26
HS31
HS33
HS17
HS15
HS18
HS27
HS16
HS30
HS32
HS20
HS21
HS14
HS19
HS22
HS13
HS12
52.5
52.5
52.5
52.5
40
40
40
30.2
30.2
30.2
8.3
8.3
8.3
8.3
8.3
5.83
Rolling 1-min
Rolling 2-min
Rolling 3-min
Rolling 5-min
Segmented
Sequential 1-min
Sequential 2-min
200
300
400
500
SH04
SH02
SH01
SH03
52.5
40
40
14.2
(b)
300
600
900
1200
mg O2 kg−1 h−1

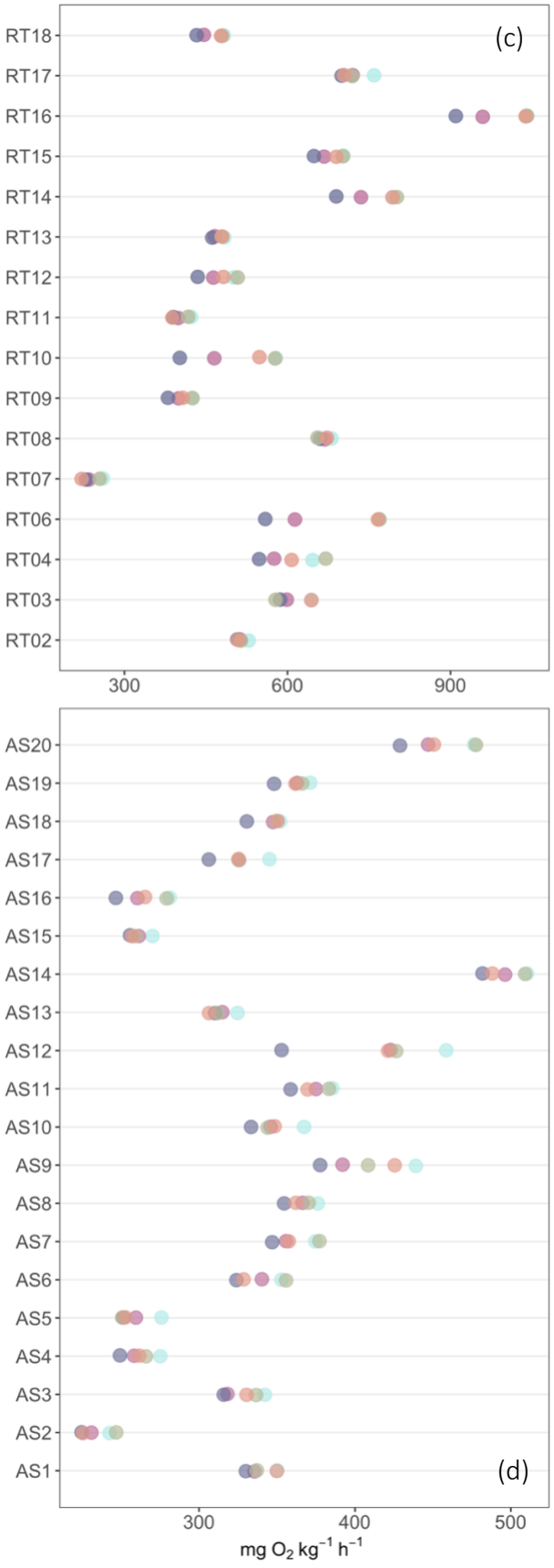
(c)
RT18
RT17
RT16
RT15
RT14
RT13
RT12
RT11
RT10
RT09
RT08
RT07
RT06
RT04
RT03
RT02
300
600
900
AS20
AS19
AS18
AS17
AS16
AS15
AS14
AS13
AS12
AS11
AS10
AS9
AS8
AS7
AS6
AS5
AS4
AS3
AS2
AS1
(d)
300
400
500
mg O2 kg−1 h−1

Figure B-1 **MMR estimates from each model varied within individuals. Individuals are plotted in order of increasing body mass ((a) California Horn Shark 0.203-4.46kg, (b) Smoothhound 0.76-1.6kg, (c) Rainbow Trout 0.06-0.11kg, (d) Atlantic Salmon 0.06-0.12kg) and correspondingly increasing chamber size for sharks. (a) Arrow indicates segmented regression MMR estimate which would have doubled if a 41s window width, rather than a 45 s window width, was allowed. Mass-specific unscaled MMR values are reported for each individual (i.e. MMR at 1kg body mass).**

B.1.3 Signal-to-noise ratio method to estimate a regression window width

We tested the effectiveness of a signal-to-noise ratio analysis method by simulating background respiration data to represent a hypothetical ideal system (Zhang et al., 2019). Within an empty respirometer chamber, the oxygen consumption signal is usually very low and stable over time compared to the system noise. This analysis method uses iteratively increasing regression window widths to compare the noise in the experimental system to this relatively low oxygen consumption signal of background respiration within the respirometer chamber. From this it estimates a minimum reliable sampling window (regression window), which can then be applied to estimate MMR using oxygen consumption data (Fig A 2).

To estimate a minimum reliable sampling window, the model begins by running a series of sequential regression models across each individual background respiration trace. Each model iteration uses increasingly larger regression windows, beginning with a short window and increasing incrementally to a set large window (we used 30 seconds to 5 minutes). For a 30-minute trace, this results in 60 30-second regression windows, decreasing to six 5-minute regression windows by the last iteration of the model. Oxygen consumption rate is estimated for each regression window for each model iteration on each background respiration trace. All estimates for each regression window width are then pooled within that window width to estimate a mean oxygen depletion rate with corresponding standard deviation (S.D.) and coefficient of variation (C.V.) of that mean. Then, all S.D and C.V estimates from all background respiration traces are pooled to estimate a mean S.D. and mean C.V for each window width, which are then each regressed as a function of window width to estimate a minimum reliable sampling window.

To test this method, we simulated 8, 15 and 22 30-minute background respiration trace data sets within a hypothetical low, medium and high variance experimental system (Fig. A 2 a-c), producing three background respiration trace sample sizes for each variance level. This allowed us to additionally test for the effect of background respiration trace sample size on the resulting minimum reliable sampling window width estimate. We ran a total of 50 tests of this model at each sample size within each variance level, resulting in a total of 450 minimum reliable sampling window estimates.

Each background respiration trace was simulated by sampling one dissolved oxygen value per second from a normal distribution with a resulting average standard error of 0.0055, 0.0115, and 0.0155 for low, medium and high variance systems, respectively. Because the real rate of background respiration in respirometer chambers varies slightly between trials, slopes of hypothetical oxygen concentration over time were sampled from a uniform distribution of -0.0002 to -0.0022 to allow slight variance between each simulated dataframe. The minimum reliable sampling window width was defined as the shortest window width for which mean S.D. was not statistically significantly different from the mean S.D at the longest tested window width (5 minutes), also known as where the window width stabilizes (Fig. A 2 d). We focused on just S.D. as an indicator because C.V estimates should only be used for data on a ratio scale or data which do not exhibit negative values. Our mean C.V. estimates were negative in some cases, due to the low signal-to-noise ratio of our simulated data, and thus unusable.

B.1.4 Results of simulation tests

The estimate of minimum reliable regression window was sensitive to the sample size of background respiration traces used to estimate it, where larger sample sizes resulted in longer window width estimates (ANOVA $P < 0.05$) (Fig A 3). There was significant variability in window width estimates across iterations of the model, however this was slightly reduced with larger sample sizes. Mean window width estimates were not significantly different across variance levels, at any sample size, and we conclude that the model was unable to detect a difference in variance between experimental systems (ANOVA $P > 0.05$).

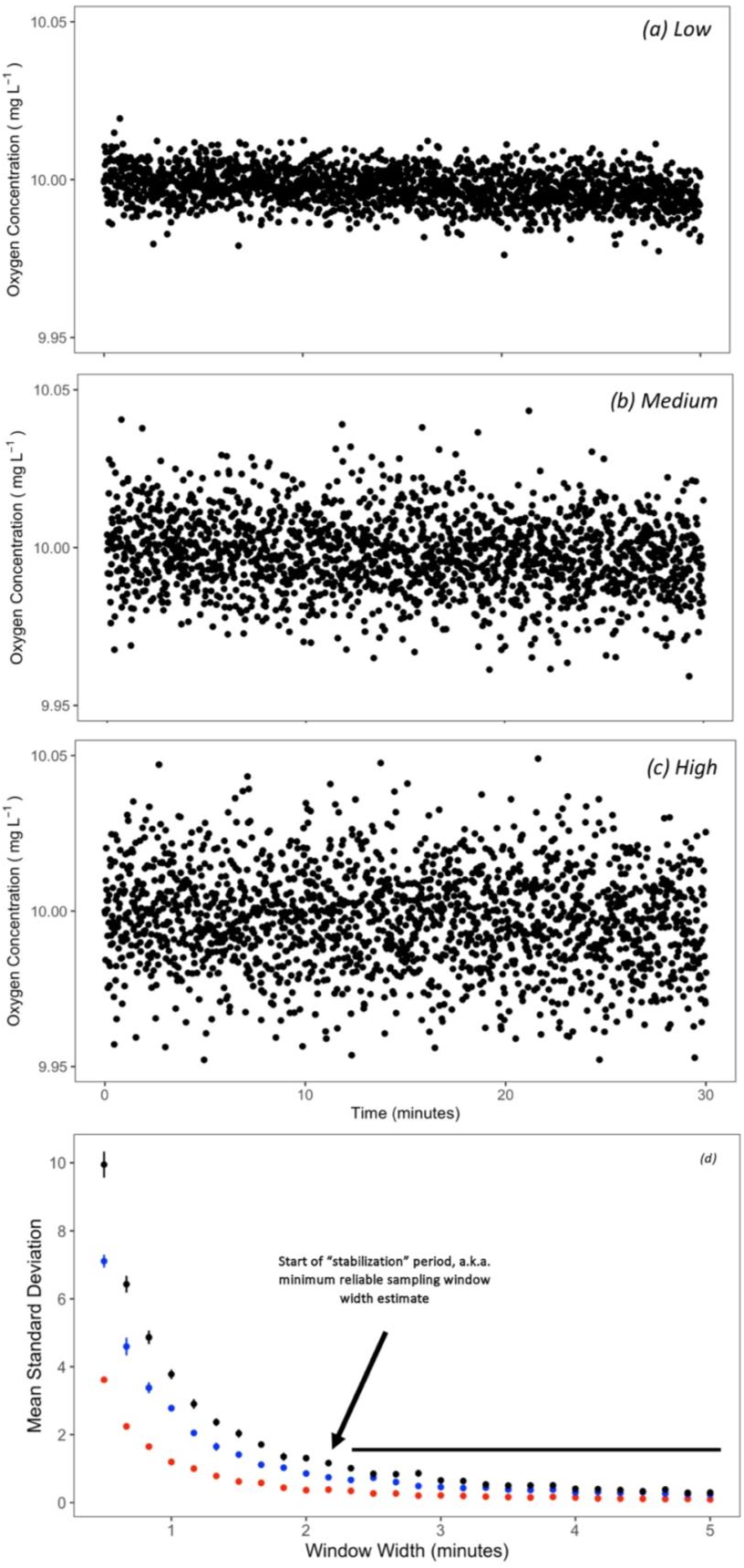
(a) Low
(b) Medium
(c) High
Oxygen Concentration (mg L^{-1})
10.05
10.00
9.95
0
10
20
30
Time (minutes)
(d)
Mean Standard Deviation
Start of "stabilization" period, a.k.a.
minimum reliable sampling window
width estimate
Window Width (minutes)

Figure B-2 **(a-c) Examples of low, medium and high variance background respiration traces simulated for signal-to-noise ratio analysis. (d) Plot of mean standard deviation at each window width (± S.E.) for one model iteration with a simulated background respiration trace sample size of 8 (high, medium, and low variance color coded as black, blue and red, respectively). Horizontal line indicates stabilized section for high-variance model, and the window width one above the first stabilized window width is designated as the minimum reliable sampling window width, indicated by the arrow.**

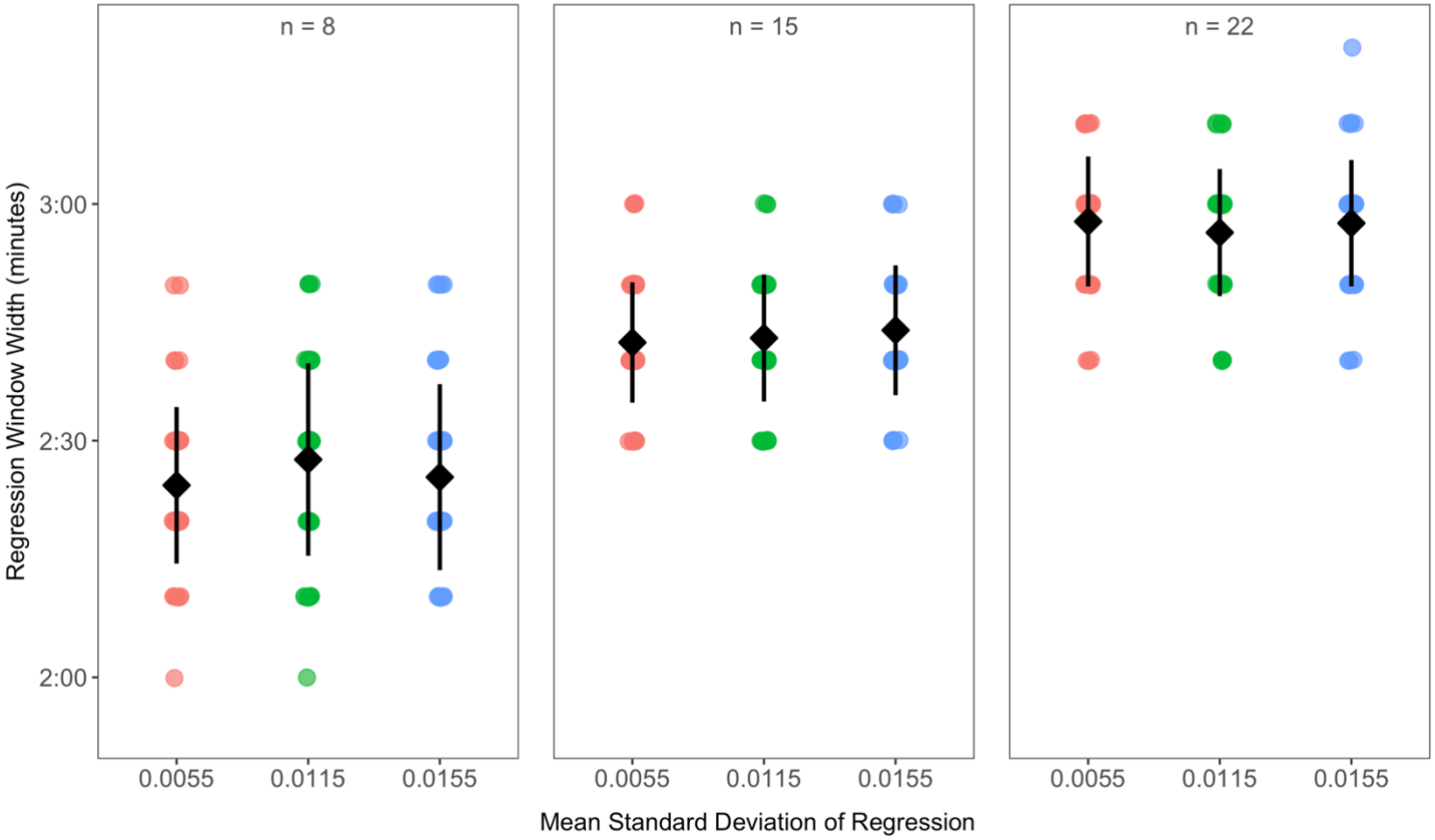

Figure B-3 **Minimum reliable regression window estimates for each background respiration trace sample size at each variance level. Fifty minimum reliable window widths were estimated to generate each distribution. Sample sizes indicate the amount of background respiration traces used to generate each minimum reliable regression window estimate (each data point). Mean minimum reliable regression window width estimates ± SD are indicated.**

B.2 References

Harianto, J., Carey, N., & Byrne, M. (2019). respR—An R package for the manipulation and analysis of respirometry data. *Methods in Ecology and Evolution*, *2019*, 1–9. https://doi.org/10.1111/2041-210X.13162

Svendsen, M. B. S., Bushnell, P. G., & Steffensen, J. F. (2016). Design and setup of intermittent-flow respirometry system for aquatic organisms. *Journal of Fish Biology*, *88*(1), 26–50. https://doi.org/10.1111/jfb.12797

Zhang, Y., Gilbert, M. J. H., & Farrell, A. P. (2019). Finding the peak of dynamic oxygen uptake during fatiguing exercise in fish. *The Journal of Experimental Biology*, *222*(12), 1–8. https://doi.org/10.1242/jeb.196568